Article

Lichenometric Analysis Applied to Bedrock Fault Scarps: The Sencelles Fault and the 1851 CE Mallorca Earthquake (Balearic Islands, Spain)

Pablo G. Silva [1,*] , Elvira Roquero [2] , Raúl Pérez-López [3] , Teresa Bardají [4] , Gabriel Santos Delgado [5]
and Javier Elez [6]

[1]   Departamento Geología, Escuela Politécnica Superior de Ávila, Universidad de Salamanca, 05003 Avila, Spain
[2]   Departamento Edafología, Escuela Técnica Superior de Ingenieros Agrónomos, Universidad Politécnica de
      Madrid, 28040 Madrid, Spain; elvira.roquero@upm.es
[3]   Instituto Geológico y Minero de España (IGME–CSIC), 28003 Madrid, Spain; r.perez@igme.es
[4]   Departamento Geología, Geografía y Medio Ambiente, Universidad de Alcalá,
      28871 Alcala de Henares, Spain; teresa.bardaji@uah.es
[5]   Departamento Ingeniería del Terreno, Facultad de Ciencias, Universidad de Salamanca, 37008 Salamanca, Spain
[6]   Departamento Geología, Facultad de Ciencias, Universidad de Salamanca, 37008 Salamanca, Spain
*   Correspondence: pgsilva@usal.es

Featured Application: The paper displays the analysis of lichen colonization of rocky fault-scarps to perform geochronological analyses and evidence ancient to historical earthquakes. This applied research shows the high sensitivity of vertical/horizontal position, geographical orientation and lithological nature of lichen colonized rock surfaces for the obtention of reliable lichen growth rates (LGR) applicable to geochronology.

Abstract: The Sencelles Fault constitutes the main extensional structure of Mallorca Island (Spain), holds a NE-SE orientation, and has been identified as the possible seismic source of the 1851 CE Palma earthquake (VII EMS.) The SE termination of the fault (Sta. Eugenia Segment) features a linear bedrock fault scarp of a maximum of 3.15 m height. The last 840 m of this rocky scarp display a significant horizontal banding, with up to five differentially weathered ribbons colonized by lichens. The lichenometric analysis is based on the measurement of 155 specimens of *Aspicilia calcarea* (*Ac*) and *Aspicilia radiosa* (*Ar*) in tombstones and funerary monuments (with inscribed dates) from the nearby cemeteries of Sta. María del Camí, Sta. Eugenia and Sencelles, to obtain the local lichen growth rates (LGR), with the two last graveyards being directly located in the fault zone. Lichens were measured on variously oriented (N, S, NE, SW, etc . . .) horizontal and vertical surfaces, generating differentially oriented lichen populations (DOLPs) to be compared with the *Ac* and *Ar* specimens colonizing the studied fault scarp (38 measured individual specimens). After successive trial and error regression tests, vertical DOLPs resulted in the best appropriate groups for the analysis, with LGR of 0.23–0.31 mm/yr. Horizontal ones reached widths of up to 20 cm, with LGR up to 0.84 mm/yr, which were clearly oversized. The application of the selected LGR points to a human-induced origin for the thin basal lichen ribbon of the scarp (10–13 cm), which should have developed during the middle 20th century (c. 1950–1966) because of documented ground leveling works. However, the second ribbon of the scarp (23–47 cm) shows exposure dates of 1852 ± 40 (*Ar*) and 1841 ± 59 (*Ac*), overlapping the date of the 1851 CE earthquake. The study is complemented with data from a fault trench excavated in the year 2002 at the toe of the scarp. The combined data of lichenometry, fault trenching, and the length of the analyzed fault scarp (c. 840 m) indicate that the studied segment of the fault cannot be considered a co-seismic surface faulting related to the 1851 CE event as a whole, but a relevant secondary earthquake effect on a pre-existing fault scarp (e.g., sympathetic ground ruptures).

Keywords: sencelles fault; lichenometry; lichen growth rates; bedrock fault scarp; 1851 CE Palma earthquake; Mallorca Island; Spain

1. Introduction

This study explores the application of lichenometric analyses to unravel the chronology of bedrock fault-scarps, where other paleoseismological techniques, commonly used in alluvial and colluvial materials, are harsh to apply. Lichenometry is a dating technique normally applied to analyze the age of glacial moraines [1,2], landslides [3], and rockfall events related to coseismic shaking [4,5]. In most cases, lichenometric analyses are applied on exposed horizontal surfaces where lichens have the most favorable growing conditions, producing large *tallus* sizes [6,7]. The pioneer works of Robert E. Wallace on differential lichen colonization and weathering of prehistoric and recent rocky fault scarps [8,9] were the only ones preliminary exploring this method. More recently, an introductory study on the Sencelles Fault applies modern approaches to lichenometric analyses of horizontal surfaces to vertically exposed surfaces of bedrock fault scarps [10]. This work points to the large variability of lichen growth rates (LGR) related not only to the vertical or horizontal condition of the exposed surfaces but also to their geographical orientation, exposure to maritime areas, etc. Consequently, the obtained regional regression curves of LGR from the measurement of lichens in graves with inscribed dates in local cemeteries are sensitive to both position and orientation, producing differentially oriented lichen populations (DOLPs).

The present work improves and completes the preliminary lichenometric analysis of rocky fault scarps on Mallorca Island [10]. The study uses data from 180 lichen specimens in three cemeteries close to the fault to be dated, two of them directly placed onto the proper fault trace. The obtained data are combined with previous unpublished fault-trench analyses to explore the relationships between the different lichen bands flooring the fault scarp and historical earthquakes on the island. The performed analysis allows us to identify recurrent displacements of the Sencelles Fault scarp based on differentially lichen colonization ribbons. Part of the youngest basal ribbon has been tentatively related to the 1851 CE Palma Earthquake ($\leq$VIII EMS Intensity) [10]. However, observed displacements cannot be truthfully cataloged as surface faulting events, but as secondary or sympathetic coseismic ground ruptures (*Sensu* Serva and de Polo [11,12]). Additionally, the performed study also develops a methodological approach based on the lichen analysis of vertically exposed rocky surfaces for rapid and low-cost geochronological studies of presumably historic bedrock fault scarps. The performed lichenometric analysis can thus date limestone surfaces as old as 700–800 years, as has been proved in the semiarid SE Spain [7,13]. This methodology can replace or complement more expensive geochemical dating techniques of rocky surfaces based on the analysis of cosmogenic isotopes [14,15].

2. Geological and Geomorphological Context

Mallorca is located in the western Mediterranean, which is the largest emerged terrain of the Balearic Promontory, which constitutes the prolongation of the Betic Cordillera into the Mediterranean basin (East Spain; Figure 1) [16]. The promontory is bounded by two large extensional structures: the "Valencia Through" to the north and the "Emile Baudot Scarp" to the south [16,17]. This last one is a c. 1 km high submarine escarpment defining the northern border of the Algerian Basin [16]. The island is internally defined by a NE-SW trending basin-and-range structure, with important extensional Neogene basins [17], such as the Palma Bay Basin, The Central Inca Basin, and the Alcudia Basin (Figure 1).

The NE-SW Sencelles Fault (SCF) bounds the Inca Basin to the south and is the main extensional structure of Mallorca Island (Figure 1). The fault has been active along the last c. 19 Ma (early Miocene), with a maximum accumulated throw of 750 m [18,19]. Modern gravity and borehole data [17] support the north-to-south half-graben model previously proposed for the Inca Basin [18–20] with the depocenter close to the Sencelles Fault (Figure 2), where the maximum thickness of Plio-Quaternary deposits (~120 m) is reached [14]. Synthetic reverse faults and antiform structures occur in the hanging wall of the SCF, affecting the entire post-tortonian sequence (Figure 2). The Messinian sequence includes a lagoon-reef complex buried by the so-called Terminal Complex (*Bonanova Fm.*

and *Santayi Fm.*). These are formed by the littoral brackish to mangrove facies grading occasionally to grey marls with gypsums attributed to the end of the Messinian [17]. The broad syncline is eventually filled by the Lower Pliocene (*Son Mir Fm.*) and the Upper Pliocene (*St. Jordi Fm.*) littoral series which are also deformed by the SCF. The fault cuts the whole Neogene sequence filling the Inca Basin, which is accommodated in a broad syncline and offset by high-angle antithetic normal faults dipping to the NW (Figure 2). These structures occasionally cut the Upper Pliocene littoral calcarenites (*St. Jordi Fm.*) (Figures 1 and 2) forming NW-wards facing bedrock fault scarps with important accumulations of Quaternary alluvial deposits (~60 m thick) at the downthrown blocks [20]. The distal alluvial deposits are back-tilted and hold fossil remains of the extinct caprine *Myotragus balearicus* (Figure 3), endemic to the island during the Pleistocene [18]. However, geophysical data indicate that the maximum thickness of Quaternary deposits in the Sta. Eugenia sector hardly surpasses 10 m, linked to the creek of Torrent de Solleric and Holocene in age [17,20].
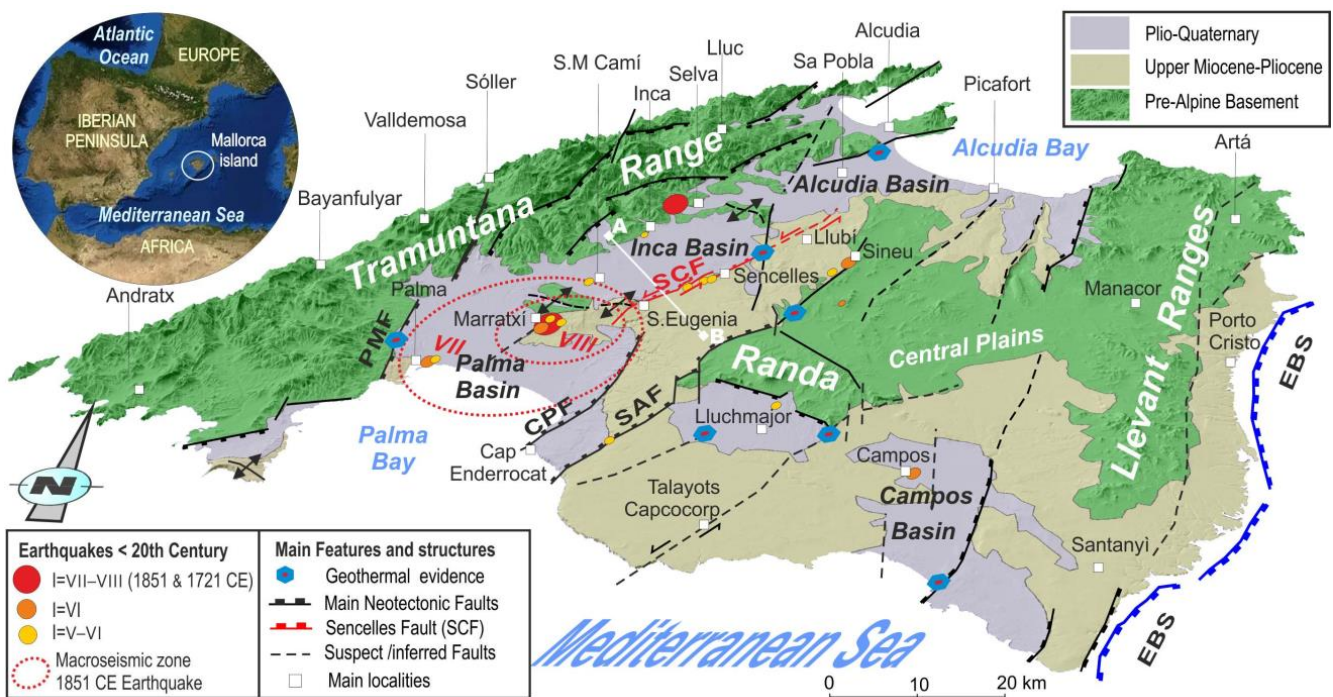

Figure 1. The geological and structural framework of Mallorca Island, showing the location of the main Quaternary basins, neotectonic faults, related thermal springs, seismic activity, and the macroseismic area of the 1851 CE Palma Earthquake (Sa Cabaneta-Marratxi). PMF: Palma Fault; CPF: Cap d'Enderrocat Fault; SAF: Sineu-Algaida Fault; SCF: Sencelles Fault; EBS: Offshore Emile-Baudot Scarp. White line: A–B location of the cross-section of Figure 2.

Consequently, geologic and geomorphologic evidence prove the activity of the SCF from Late Pliocene to recent times with a mean throw of around 100 m for the last ~3 Ma [20]. This fault (7 km long) has been subdivided into two main segments based on their structural and geomorphological features [20]: The Sencelles and the Sta. Eugenia segments are separated by the rock salient of Puig Son Seguí (Figure 3). However, some authors lengthen this fault 6 km to the NE in a poorly defined third section (Llubí Segment), where the fault displays a suspect dominant left-lateral strike-slip behavior [21] and generates a small pull-apart basin (Figure 3). In any case, although the fault displays some strike-slip features (e.g., rock salients, sag ponds, die-out anticlines; Figure 3), its overall geometry and kinematics at the surface fit better to that of the normal fault scarps described in the literature [8,9,12,15]. This study is focused on the easternmost segment of the fault (Sta. Eugenia Segment), with a length of about 2.8 km between the rock salient of Puig Son Seguí

and Sta. Eugenia (Figure 3). This fault segment has been the subject of geomorphological and palaeoseismological studies in relation to the analysis of historical seismicity in Mallorca, and in particular to the 1851 CE Palma Earthquake (VII EMS; VIII ESI07) [20,22,23]. The SW termination of the Sta. Eugenia segment is featured by a NE-SW bedrock fault scarp facing the NNW (Figures 2 and 3). The scarp is developed on Plio-Pleistocene cemented calcarenites of the *St. Jordi Fm* [19], reaching a maximum height of 3.15 m to the west in the zone adjacent to the rock salient of Puig Son Seguì (Figure 3). The height of the scarp declines progressively to the east until it dies out under the cemetery of Sta. Eugenia (Figure 3). The last 840 m of the scarp displays a strong horizontal banding because of differential weathering and lichen colonization [10,20] with a basal and younger ribbon almost free of lichens (Figure 4).
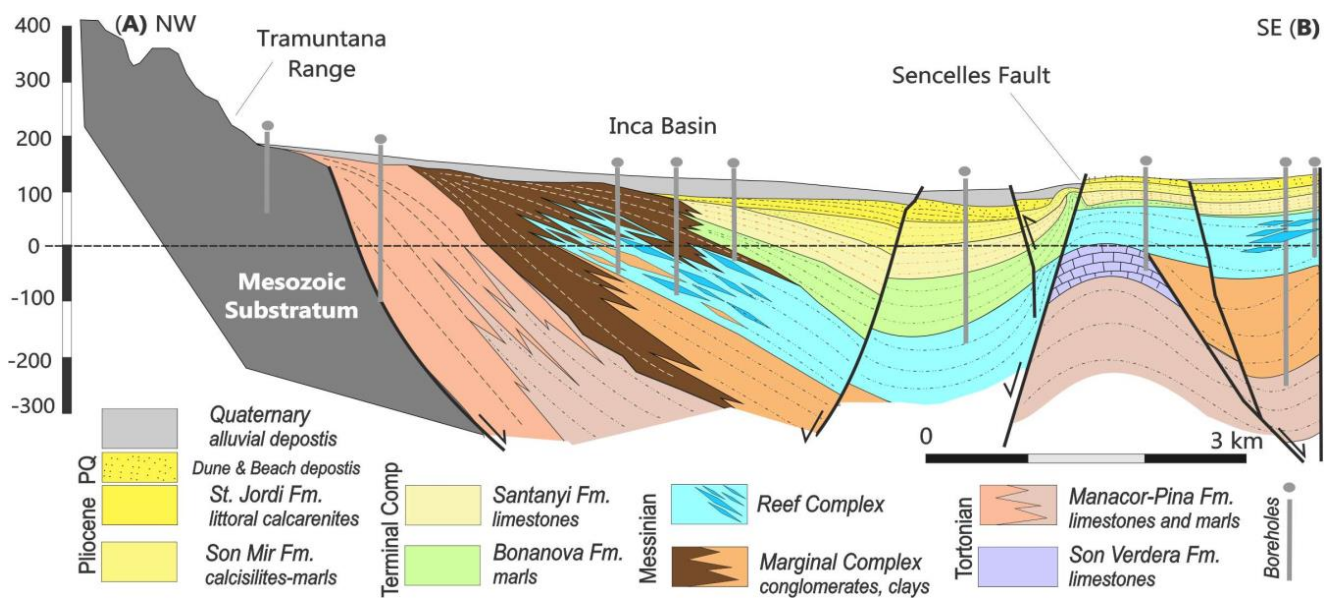
Figure 2. Schematic NW-SE cross-section of the Inca Basin based on geophysical and borehole data from the works of Capó and García, 2019 [17]; Benedicto et al., 1991 [18] and Silva et al., 2001 [20]. See Figure 1 for location of cross-section (**A**,**B**).

This study aims to improve and complete former lichen analyses [10], complementing them with a previous fault trench survey [23] to unravel the chronology of the bedrock fault scarp and to establish the potential relationships with the 1851 CE earthquake. This earthquake is the strongest seismic event that has ever struck Mallorca Island, and is very well described in contemporaneous historical reports [24–26] as well as in epoch newspapers compiled by Silva et al. [20].
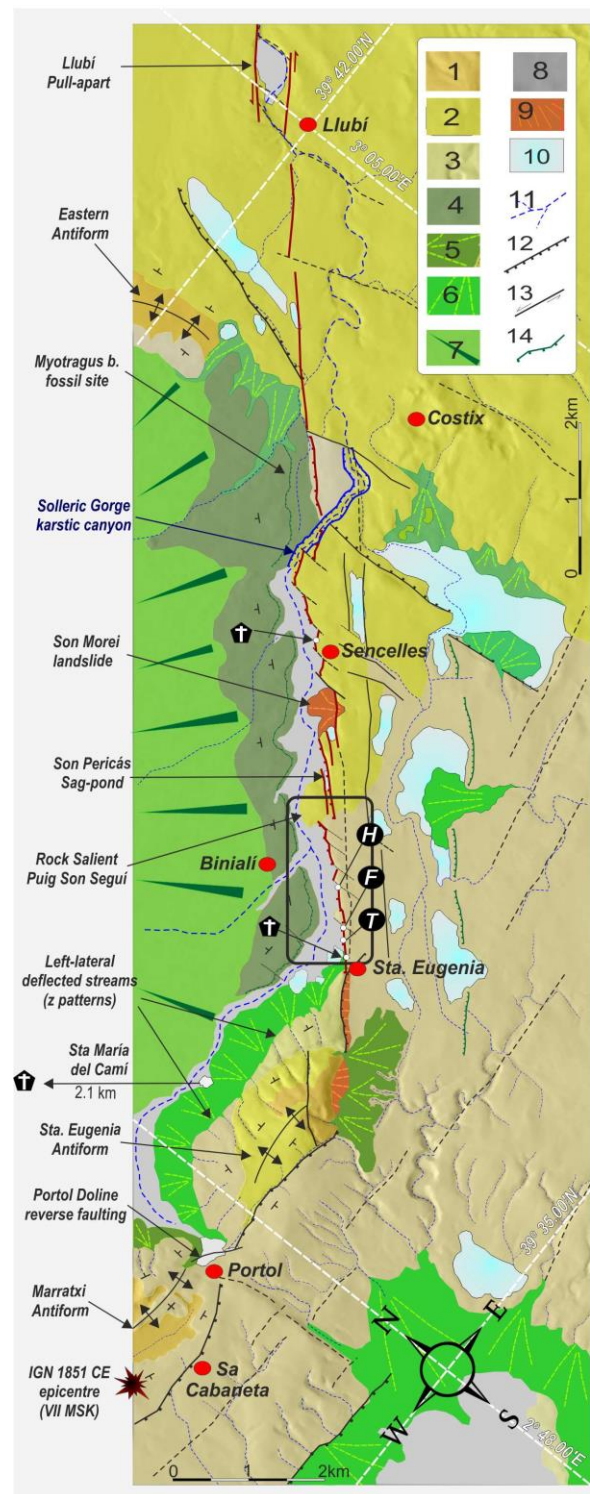
Figure 3. Schematic strip-map of the Sencelles Fault showing its most relevant features. 1—Pre and syntectonic materials (pre-Serravallian); 2—pos-tectonic pre-Pliocene materials (Serravallian to Messinian); 3—Plio-Quaternary materials (*St. Jordi Fm.*); 4—Lower-Middle Pleistocene alluvial materials (Inca Basin); 5—Middle Pleistocene alluvial fans with crusted surfaces; 6—Late Pleistocene-Holocene alluvial fans; 7—distal (sheet flood) fan Holocene deposits Inca Basin; 8—Holocene valley fillings (Solleric stream); 9—Colluvial deposits and landslides; 10—Pleistocene to Holocene Doline and pond deposits; 11—Drainage network; 12—Normal faults; 13—Strike-slip faults; 14—Morphostructural escarpments. T: 2002Trench site; H: Destroyed House site (lichenometry); F: Stone Fence (lichenometry Red dots: main localities. Crossed black pentagons with white crosses (analyzed cemeteries).

Figure 4. The Sencelles bedrock fault scarp at the central sector of the Sta. Eugenia Segment. (**a**): Oblique view showing the rocky free face of the fault scarp in the year 1998 (Fence Site; F in Figure 3). (**b**): Detailed frontal view of the scarp displaying the different ribbons analyzed in this study during the year 2015 (House Site; H in Figure 3).

3. Materials and Methods

The main methodology used in this study is basically lichenometry, largely applied in archaeometry and geomorphology to date events in exposed rocky surfaces [1,2,7]. The purpose of this technique is to obtain the annual growth rate of a given species by calculating its lichen growth curve (LGR) through its calibration on surfaces of known age and applying it to the lichens found on the rock surface to be dated [27]. This process requires repeated and multiple measurements of the maximum diameter of the lichen body (*thallus*) of the selected species on different rock surfaces [1,6,7,27]. We selected *Aspicilia radiosa (Hoffm.)* and *Aspicilia calcarea (Linn.)*, two well-known disk-shaped crustose lichens and very common in calcareous rocky surfaces. Both species present a pseudo-circular shaped *thallus*, easy to measure and already used as "clock-lichens" both in the semiarid SE Spain [5,7,13] and in Mallorca Island [10]. Both lichens are conspicuous in the calcareous Neogene rocks around the studied zone, as is the case of the analyzed rocky scarp (Figures 4 and 5), but also in stone buildings, monuments, and tombstones built with these calcareous materials around the area.

Other lichen species present in the analyzed scarps, such as the crustose orange lichen *Xantoria clacicola* and unidentified "*foliacea*" black lichen colonies were not analyzed due to their amoeboid-like growth by the coalescence of *thallus* and the difficulty to distinguish individual *thallus* for measurement (Figure 5). These coalescent colonies are common in the upper oldest part of the scarp, but almost absent in its more modern basal portion, which is almost free of lichens (Figure 4).
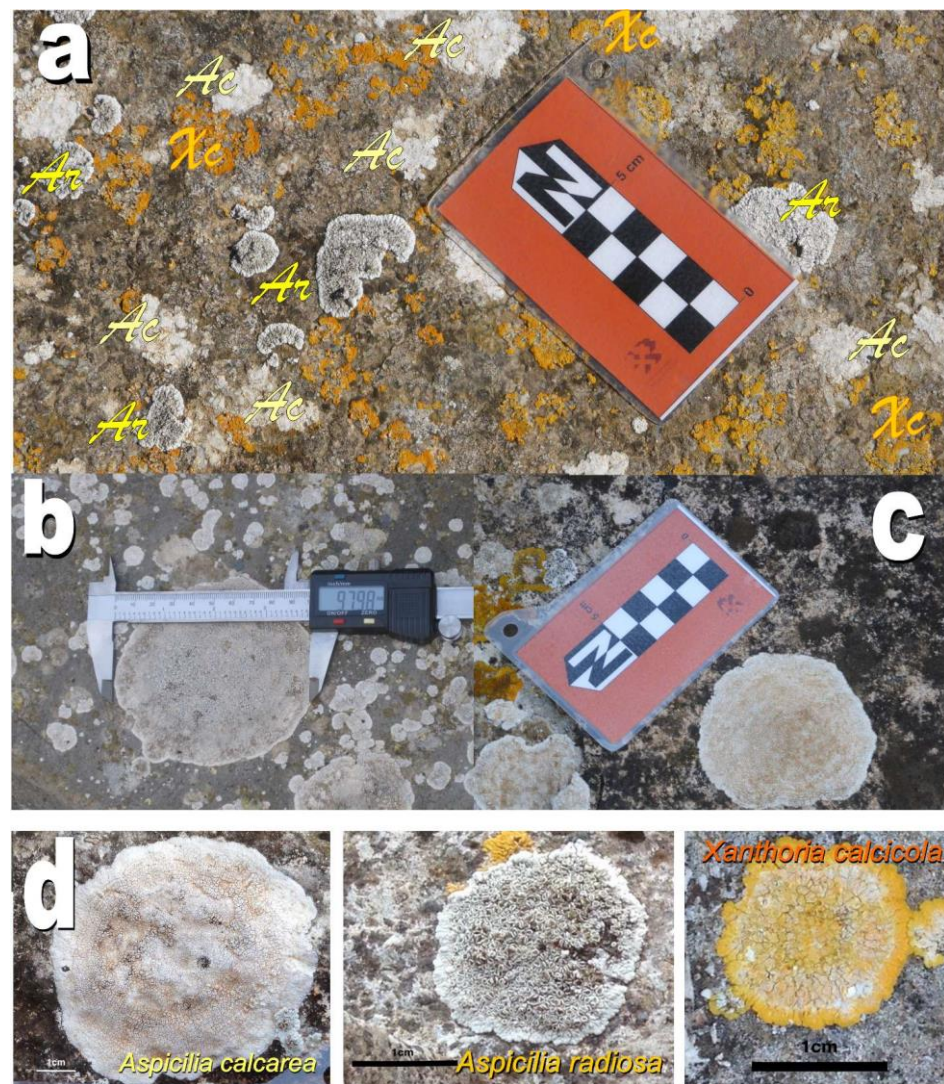
Figure 5. Examples of different lichen species analyzed in this study. (**a**): Tombstone colonized by thallus of *Aspicilia calcarea* (*Ac*); *Aspicilia radiosa* (*Ar*) and fragmented colonies of *Xantoria calcicola* (*Xc*); (**b**) half-thallus of *Aspicilia calcarea* measured with digital caliper on the Sencelles fault scarp; (**c**) complete *thallus* of *Aspicilia radiosa* in the Sencelles fault scarp. (**d**) Digital library examples of studied lichen species.

3.1. Data Collection Procedures

Measurements were carried out with "vernier-type" digital precision calipers (Figure 5). Five different measurements of the maximum *thallus* diameter were taken for each specimen, obtaining an automatic average sizing by the digital device. Besides the maximum diameter, each measurement was identified by (a) the name (where possible); (b) the date quoted in the tombstone (mausoleum wall or funerary monument); (c) the horizontal or vertical position of the analyzed surface; and (d) geographical orientation (North, South, etc.) taken with a compass. This protocol subsequently enabled us to distinguish among different lichen populations according to their position and geographical orientation. Similar procedures and protocols were followed for the measurement of lichen *thallus* in the analyzed bedrock fault scarp where 38 data were collected.

A total of 180 lichen specimens were measured in tombstones, mausoleums, and funerary monuments from three different cemeteries, being clustered into several populations after the lichen species, graveyard, horizontal or vertical position, and geographical orientation. The analyzed graveyards were close to the localities of Sta. Eugenia (51 *thallus*),

Sencelles (54 *thallus*) and Sta. Maria del Camí (75 *thallus*) (black pentagons in Figure 3). The lichen spreadsheet data from the analyzed cemeteries and bedrock fault scarp are included in the annexes and complementary data. Figure 6 shows an example of data collection protocol and the resulting rose diagram of orientations for vertical and horizontal measurements taken in the Sta. Eugenia cemetery, which is located on the western termination of the fault trace (Figure 3).
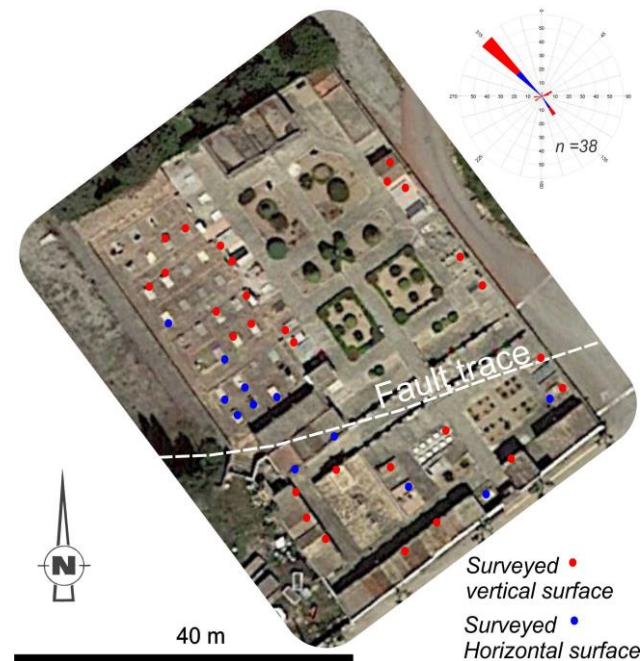

Figure 6. Example of measurement of lichen *thalli* in the Sta. Eugenia graveyard. Plots of horizontal (blue) and vertical (red) measured surfaces indicate the analyzed tombstone or mausoleum in which more than a lichen thallus might be measured. Scale numbers of the rose diagram (top right) indicate the percentage (%) of the total number of specimens measured in that locality. Vertical image from Google Earth (updated November 2021): https://earth.google.com/web/, accessed on 3 March 2023.

The maximum possible number of specimens was measured in similarly exposed vertical surfaces from all cemeteries to that of the rocky scarp to be dated (Figure 6). The Sta. Eugenia and Sencelles cemeteries are topographically conditioned by the NW-SE fault scarp, the last one is divided into two sectors (upper and lower) separated by the proper fault scarp, which is covered by a large staircase. Most of the tombstones and mausoleums in these cemeteries are oriented parallel or perpendicular to the fault trace (Figure 6). This orographic conditioning of burials is a typical feature of small foothill localities of Mallorca [28], making easier our research in these cemeteries. However, this was not the case for the Sta. Maria del Camí cemetery, located on the central plains of the Inca Basin (Figures 1–3), where tombstones and burials do not have any topographical constraints, showing an important dispersion of orientations, but prevailing those with the typical E-W orientation of catholic cemeteries.

3.2. Selection of Analyzed Surfaces and Age/Date Records

Another important factor considered to select the cemeteries to be surveyed is the time period covered by the tombstones or stone monuments to analyze. In our case, focused on the 1851 CE Palma Earthquake, we should collect data covering a similar time period. In this sense, the historical Spanish casuistic on burials also facilitates this subject (matter), since cemeteries started to be moved outside the cities and villages from the end of the 18th century. This was ordered in a Royal Edict of Charles III of Spain in 1787 CE to prevent the effects of the cholera pandemics that ravaged southern Europe at that time [29].

However, the political situation in Spain after the Napoleonic wars and the repeated cholera pandemics delayed the implementation of the royal edict until the years 1814–1865 through successive public health rulings delivered by King Charles IV and the "Cortes de Cádiz" [29]. So, the cemetery of Palma City started to move outside the urban area in 1814, but in the rest of the villages, this did not occur until 1833 to 1865 [29,30], overlapping in time with the 1851 earthquake. In this sense, the oldest collected dates in the surveyed cemeteries are from 1843 (Sta. Eugenia), 1850 (Sencelles), and 1889 (Sta. María); while the most recent dates collected in all these cemeteries range between 1970 and 1980. More recent burials are made of exotic stone materials coming from outside the island (granites, marbles, etc.), concrete, or they do not have inscribed dates. Figure 7 shows different examples of lichen populations in some of the rocky funerary structures measured in this paper to obtain LGRs.

Figure 7. Examples of lichen populations in some of the rocky funerary structures measured in this paper to obtain LGRs. (**a**) Grave of Mr. Antonio Borrás Casò and Sons (year 1956) in Sta. María del Camí; (**b**) Grave of Mr. Pedro Ferré Dols and Family (year 1938) in Sencelles with magnified inscription date; (**c**) Funerary Monument of the grave of Mr. Rafael Jaume Matas (year 1912) in Sta. María del Camí with magnified inscription date; (**d**) Mausoleum of Mr. Juan Castell and Family (year 1853) in Sta. Eugenia with magnified inscription date; (**e**) Pedestal stone -Plinth- of a cross monument at the entrance to the old cemetery of Sencelles (year 1897) with a magnified inscription date.

3.3. Obtention of Lichen Growth Rates for Dating

The technique of obtaining ages from lichen growth is based on two main assumptions [1,2]: (a) lichen growth rates can be determined throughout time using analytic methods; and (b) some lichens have circular shapes and circular growth rates. Hence, the growth rate of lichens follows a mathematical function, with a linear, power-law, exponential, or polynomial fitting [2,6,7,27]. The second assumption recognizes the possibility of obtaining lichen growth rates (LGR) from the measurement of specimens growing in rocky surfaces of known exposure time and the first one assumes that this growth rate can be fitted to a mathematical function. The selected lichen species used to calibrate and obtain a LGR is called "clock-lichen" [6,7]. Hence, we can discriminate between clock lichens with the potential to be used as a chronological tool and other lichen species useful for determining the ecology of the observed lichen sets and their relationship with local climate conditions.

In this work, we tested multiple statistical analyses for the complete set of measured lichens in the cemeteries of the zone, but also for individual cemeteries. For each test, we first checked the analysis of separated populations of the two selected clock lichens, and in a second step populations of vertical and horizontal were discriminated. Eventually, we segregated vertical populations with different geographical orientations giving place to several sets of differentially oriented lichen populations (DOLPs). Linear and power-law functions resulted in the best-fit regression equations with correlation coefficients (R^2) above 0.8 for all the DOLPs. Given the similarity of results between power-law and linear regressions, we used the simplest linear functions to calculate growth rates in mm/yr and exposure ages of the rocky scarp. Therefore, we assumed a constant linear growth rate for *A. radiosa* and *A. calcicola*.

Once we obtained the LGR function, its regression curve allowed us to date the moment when the selected clock lichen colonized and started to grow on the rock surface [7,27]. The selected lichens and the selected rocky materials can provide confident age data for the last 700–800 years in the best-case scenario. After that, large coalescent colonies of ameboid shape cover the calcareous materials, the rock surface begins to flake [7,31], and intense chemical weathering starts to carve important solution pits, as has been described in bedrock rock scarp of similar lithology [9]. In these situations, the exposed rocky surfaces are renewed, but the increasing roughness and secondary products of chemical weathering can induce significant geochemical changes in the rocky surface, favoring its colonization by other different lichen species [31]. In our case, this problem affects the upper rugged section of the scarp, but no to the basal part tentatively related to the AD 1851 earthquake [10] (Figure 4).

Another minor problem is setting the colonization time of the lichen, that is, the time that takes a lichen to colonize a rocky surface, which in most cases remains unknown [7,27]. However, this period is normally considered to be a minimum of 4–5 years for *calcicola* crustose lichens in continental and Mediterranean climates [2,5,13]. In our case, all the regression functions were adjusted considering an origin lichen (control) in the year 2011 (five years before the last field survey in 2016) with a size of 1 mm. This datum comes from the minimum LGR preliminary established for the Sta. Eugenia cemetery [10] and recalculated for all the studied cemeteries in this paper Table 1).

4. The Sencelles Bedrock Fault Scarp at the Sta. Eugenia Segment

Lichenometric analyses of the bedrock fault scarp was carried out at two different sites, both located less than 400 m away from the trench site excavated in the year 2002 [23] and from the Sta. Eugenia Cemetery (Figure 3). A total of 47 thallus measurements were taken, 32 specimens in site 1 (destroyed house site; H in Figure 3) and 15 specimens in site 2 (stone fence site; F in Figure 3) adjacent to the trench site (T in Figure 3). The best-represented lichen species was *Aspicilia calcarea* with 35 measurements, whilst for *Aspicilia radiosa* we only identified 13 specimens suitable for measurement. The fault scarp profile displayed in Figure 8 was extracted from the detailed 3D digital terrain model and a topographic map

(centimeter scale) performed in the zone by Silva et al. in the year 2001 [20]. The position and relative size of the analyzed thallus of both species, taken on the two analyzed sites, are projected in this profile.
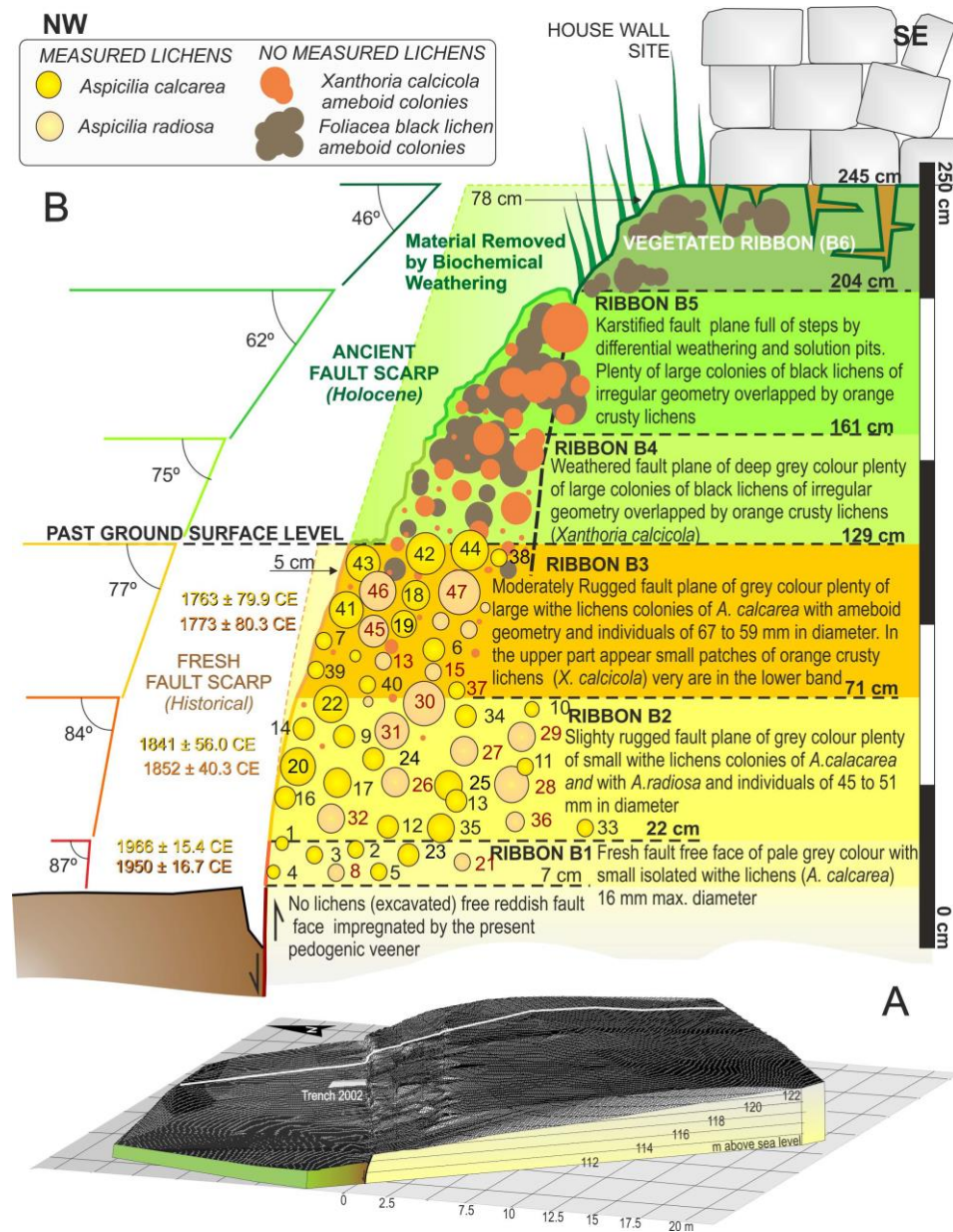

Figure 8. Morphometric and lichenometric features of the bedrock fault scarp at the Sta. Eugenia Fault Segment. (**A**) 3D Digital elevation model (5 cm pixel) of the fault produced by GPS topographic measurements in the zone of the excavated trench in 2002 and Site 1 (Stone Fence; F in Figure 3). (**B**) Synthetic profile of the Sencelles bedrock fault scarp in Site 2 (Destroyed House; H in Figure 3) illustrating the different lichen ribbons analyzed in this paper. Measured Lichen species are plotted to attend to their position in the fault plane, with equivalent sizes (larger or smaller circles). Mean angles of the fault plane bands and ribbons, the position of lichen ribbons above the present ground surface (cm), theoretical width of removed materials by biochemical weathering and mean computed ages (age 2 in Tables 2 and 3) from the obtained LGR functions for the three lower ribbons are displayed.

The westernmost 840 m of the Sta. Eugenia fault segment features the development of differentially weathered ribbons characterized by the colonization of diverse lichen species and different lichen sizes. Lichen colonization clearly decreases from the top to the base of

the scarp-free face, which is nearly free of lichens. Considering the intensity of weathering onto the exposed fault plane, two prominent bands, one above the other, are preserved in the near-planar surface of well-cemented calcarenites. These are interpreted as fresh and ancient fault scarps (Figure 8), displaying yellowish and greenish colors, respectively (Figure 4). The basal band displayed a slightly rugged 1.29 m wide surface (fault plane) with a dip angle decreasing from the base to the top of the free face from 87° to 77° degrees. This younger band is differentially colonized by the studied lichen species (*A. calcarea* and *A. radiosa*), with upwards-increasing density and downwards-decreasing size, but arranged in three different ribbons (Figure 8). The basal ribbon B1 (7 cm wide) only presented a few small patches of lichens less than 20 mm in size (Figures 4 and 8). On the contrary, the upper ribbon B3 was densely colonized and lichens coated more than 40 percent of the surface (Figure 4). The intermediate ribbon B2 displayed an intermediate stage of colonization, with less than 25 percent coated by lichens. This intermediate B2 band has been tentatively linked to the 1851 CE Palma earthquake (VII EMS) by previous studies [10,20].

In contrast, the upper band of the scarp showed evidence of long-term exposure produced by earlier fault displacements. This band is very rough, and significantly pock-marked by solution pits. It is colonized by coalescent colonies of *Aspicila*, but mainly of the crustose orange lichen *Xantoria calcicola* and unidentified "*foliacea*" black lichens. Curiously, this band presented lesser lichen coating (density) than the upper part of the basal band (Figure 4), which can be explained by the exfoliation effect of weathering and flaking of the exposed rocky surface mentioned above [31]. This band is about 1.16–1.20 m wide and it is separated from the lower band by a small rocky step related to scarp retreat by weathering (Figures 4 and 8). Although in a discontinuous way, this rocky step appears throughout the 840 m length of the Sta. Eugenia segment. In several zones, the upper band is eroded by small V-shaped rills carved in the fault plane (Figure 4a). These rills end at the mentioned rocky step, being perched from the present ground surface above the more fresh fault plane (lower band). Both features (rocky steps and perched rills) can be interpreted as the consequence of the long-term weathering of the upper band of the scarp, evidencing the position of a relatively stable ancient ground surface during prehistorical times. Morphometric measurements illustrated in Figure 8 indicate that the scarp retreated 83 cm by weathering from the lower band (5 cm) to the upper band (78 cm), generating a roughly convex stepped slope (Figure 8). These classes of stepped slopes are typical of scarp retreat processes by chemical weathering during repeated exposure events triggered by climate (erosion, exhumation) or more commonly by recurrent ground failures (gravity, earthquakes) [31–34]. On the other hand, the perched rills of the upper band strongly suggest that the intervening exposure event between the lower and upper bands of the scarp was abrupt. Considering that we were analyzing a fault scarp, we focused on a tectonic scenario wherein these two bands of the scarp might represent two evolutionary historic (lower) and prehistoric (upper) stages of the bedrock–fault scarp. The roughness, dimensions of the solution pits, density of lichens, and upwards-decreasing dip angle (75–46°) of the exposed surface allow differentiating another two ribbons in the upper band (Figures 4 and 8). This also suggests at least another two different recurrent displacements assembled in this prehistorical band of the scarp. When compared with the morphometric properties of other bedrock fault scarps [33–35], the roughness, deep weathering stage, and retreat angle of this degraded band of the scarp suggest a Holocene age. These features are similar to those shown by the exposed surfaces of the megalithic structures named Talayots in the Balearic Islands (e.g., Capcocorp Vell; Figure 1) dated around 1200–1500 years BCE [10]. This suggests that the upper ribbons of the Holocene scarp might have an age older than c. 3500 years BP.

A last (and older) sixth ribbon can be differentiated in the upper 40–45 cm of the scarp (Figure 8). This top ribbon is densely vegetated, karstified, and strongly pockmarked by solution pits, constituting a very rough surface unsuitable for lichen analyses. Its top constitutes the degraded crest of the scarp limiting the upper pre-faulting original surface in the southern footwall of the SCF carved into the Plio-Quaternary calcarenites (Figure 3).

In this case, the scarp toe does not record the original lower pre-faulting surface (*sensu* Wallace) [32]), since it is buried by a thick colluvial and alluvial cover [20–22]. Geophysical and borehole data [17,20,35] from the downthrown block adjacent to the SCF indicate that the top of the faulted Plio-Quaternary calcarenites can be found at depths between 60 and 100 m (Figure 2). These data suggest an important activity of the fault throughout the Quaternary period, generating a wide accommodation space for the alluvial sediments coming from the Tramuntana Range to the North.

5. Lichen Growth Rates: LGR Curves for the Zone

Following the methodological approaches described in Section 3 (Materials and Methods), we selected three cemeteries in the environs of the studied fault scarp to obtain lichen growth data from stone elements with inscribed dates (tombstones, mausoleums, and funerary monuments). Multiple measurements of the selected species were taken in the cemeteries of Sta. María del Camí, Sencelles and Sta. Eugenia (Figure 3), discriminating horizontal and vertical populations with different geographical orientations. The plotting of the gathered data in XY graphics results in a large dispersion suggesting the need for further separated analyses for specific populations by cemetery, lichen species, vertical/horizontal position, geographical orientation, etc. In total, 180 data on lichen size were collected for individual specimens of the analyzed species. The gathered data cover a period of c. 140 years, from 1853 to 1992 CE, within the range of the elapsed time since the last strong earthquake in the zone (1851 CE Palma Event).

As displayed in Figure 9, the plotting of the complete dataset of measured specimens showed a large dispersion, producing a poor correlation (R^2 < 0.51), but suggesting a clear split between *A. radiosa* and *A. calcarea* populations (Figure 9a). On the other hand, correlations for the different analyzed cemeteries also displayed clear differentiation in the LGR between vertical and horizontal lichen populations (Figures 9b and 10. The regression graphics in these figures do not show the 180 measured specimens, but the greatest lichen sizes obtained for different dates (simplified to years) in the analyzed cemeteries. In all these sites, the differentiation between the growth rates of vertical and horizontal lichens population is clear. The Sta. María cemetery (Figure 9b) showed the maximum dispersion for a site, as well as the fastest LGRs with low-angle regression lines. However, LGRs for horizontal populations (0.56–0.84 mm/yr) were significantly larger than those for vertical ones (0.36–0.48 mm/yr). These LGRs nearly duplicated or triplicated those obtained for the Sta. Eugenia and Sencelles cemeteries (Table 1).

The performed analyses for the two lichen species indicated a strong sensitivity of LGRs to vertical/horizontal position, orientation, and location, but LGRs of horizontal populations are higher (near duplicate) than those of the vertical ones, as expected (Table 1). The results obtained from the different cemeteries are clearly decoupled, as was highlighted by preliminary lichenometric analysis on the island [10] and despite the proximity of the analyzed cemeteries (c. 6 km apart from each other). This is especially significant when comparing the data from the Sta. Maria and from the Sta. Eugenia and Sencelles ones. These two last graveyards, located on the fault trace, are topographically protected (from winds) by the antiform reliefs of Sta. Eugenia and Marratxi in the southern sector of the Inca Basin (Figures 1 and 3). On the contrary, the Sta. Maria graveyard is in the central sector of this Basin with an important exposure to the northerly dominant tramontane winds (NNE) and sunlight. Besides that, the significant N-S rainfall gradient triggered by the orographic effect of the Tramuntana Range favor the differential growth of lichens (Sta. María mean annual rainfall rates of around 535 mm versus 430 mm in Sta. Eugenia [10]). In addition, the geographical orientation of exposed surfaces clearly favors the increase of LGRs in NW-oriented surfaces, facing the dominant Tramontane winds. Considering these constraints, the analysis developed in this study is mainly focused on vertical lichen populations, N-NW oriented in the cemeteries of Sta. Eugenia and Sencelles, following a similar scheme to the analyzed fault scarp. Data from Sta. María were discarded since they presented higher LGR values (Table 1) not representative of the fault scarp zone.
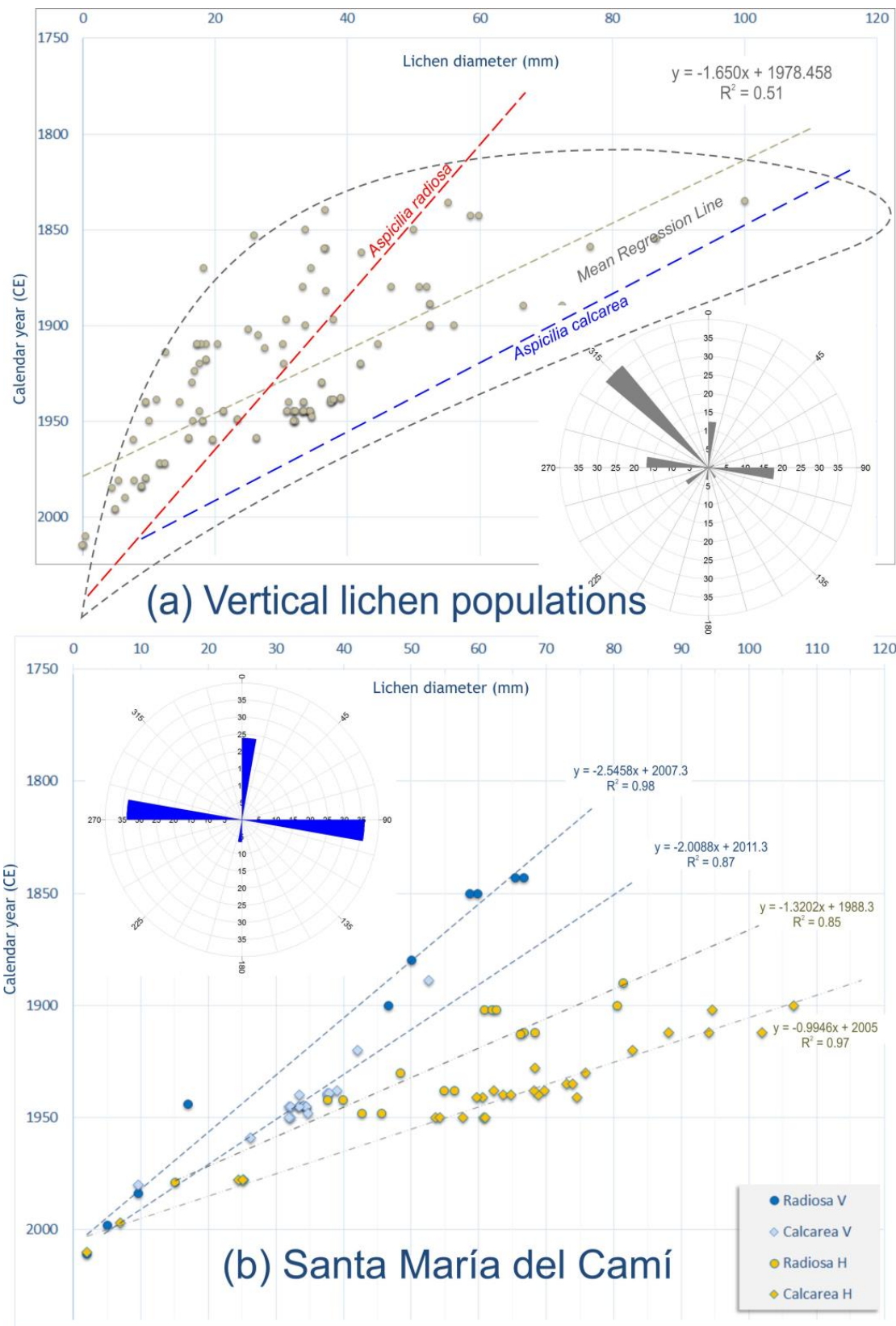
Figure 9. XY dispersion graphics showing the best-fit linear regression lines and corresponding equation for selected vertical populations of lichens from the three cemeteries (**a**) and the cemetery of Sta. María del Camí within the Inca Plain displaying vertical and horizontal lichen populations (**b**). Rose diagrams show dominant orientations of the measured lichen specimens.
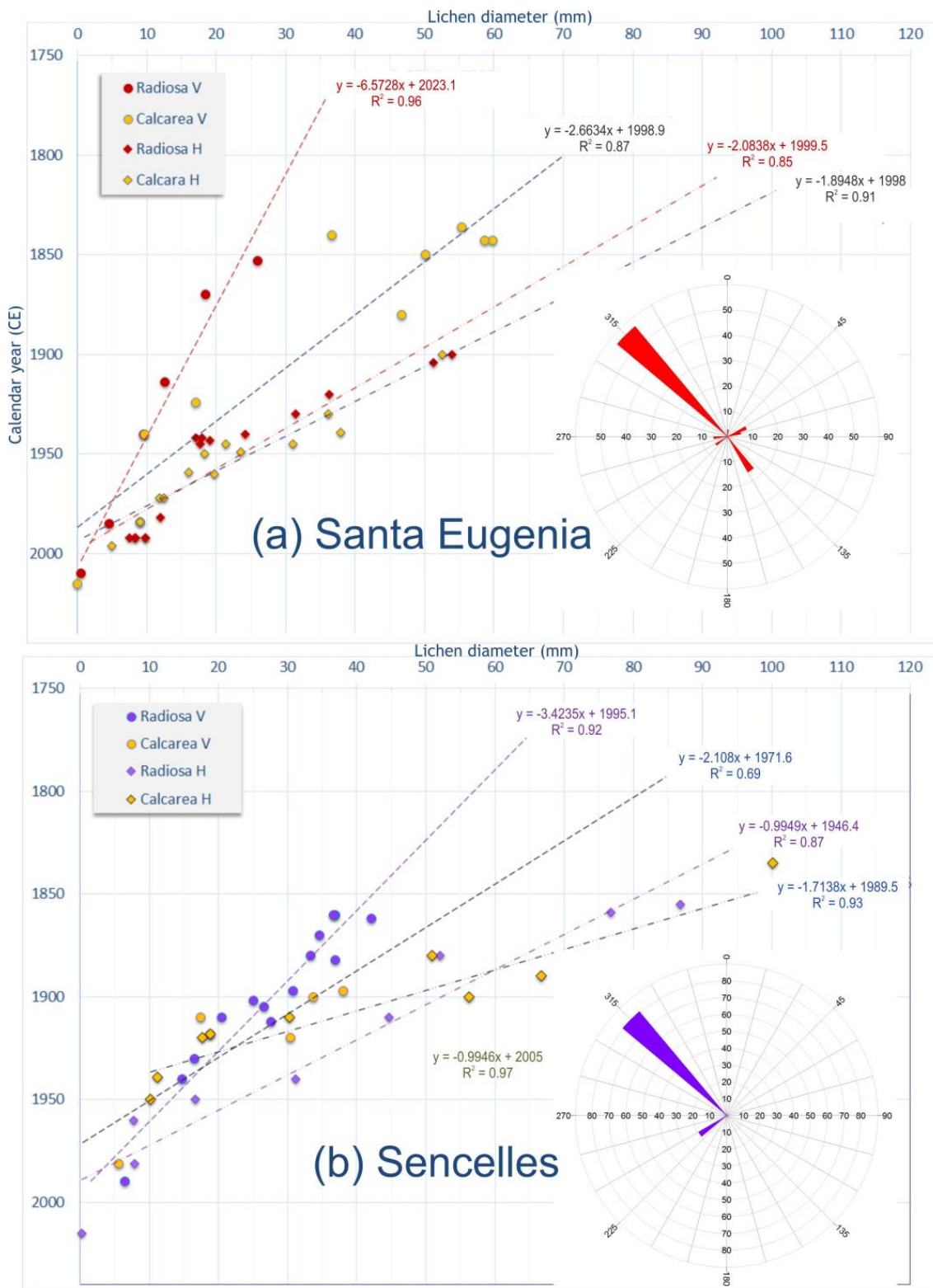
Figure 10. XY dispersion graphics showing the best-fit linear regression lines and corresponding equations for vertical (V) and horizontal (H) lichen populations in the cemeteries placed on the trace of the Sencelles fault. Rose diagrams show the dominant surface orientation of the measured lichen specimens.

In this way, the more suitable populations for this study are those found on vertical surfaces from the Sta. Eugenia and Sencelles cemeteries with a N-NW orientation, which in

fact are the more abundant ones (Figure 10). The vertical populations of *A. radiosa* result in mean LGRs of 0.14–0.19 mm/yr, whilst those of *A. calcarea* are of 0.23–0.30 mm/yr. On the contrary, horizontal lichen populations show LGRs up to 0.26 mm/yr for *A. radiosa* and 0.35 mm/yr for *A. calcarea* (Table 1). These LGRs are slightly higher than those proposed for *A radiosa* in SE Spain (0.25 mm/yr), where annual rainfall rates are lower (c. 360 mm/yr) [5,7,13]. In our study, the Mausoleum of Mr. Juan Castell (1853 CE) and the tombstone of Mr. Bibilon Armengual (1850 CE) provided specimens of larger size in vertical (42.6 mm) and horizontal (59.8 mm) surfaces, respectively. In Sencelles, the stone pedestal of a large iron cross from 1897 CE in the lower part of the cemetery provided the largest lichen sizes for horizontal (101.7 mm) and vertical (42.9 mm) populations (see Figure 7). Besides obtaining mean numerical LGRs from the direct relationships between lichen size and inscribed dates, all the analyzed populations were subjected to statistical analyses to obtain mathematical functions describing annual lichen growth (Tables 2 and 3). In all cases, we selected the simplest best-fit linear regressions with correlation rations (R^2) over 0.8 and in many cases up to 0.95 (Figure 10).

Table 1. Summary of lichen measurements in the analyzed cemeteries indicating the year of the oldest analyzed tombstone, maximum lichen sizes, and resulting mean LGR.

Site	Position	Lichen Specie	*Thallus* Number [1]	Oldest Year	Max Size (mm)	Max LGR (mm/yr)	Mean LGR (mm/yr)
Sta María	Horizontal	*A. radiosa*	10	1855	81.38	0.73	0.56 ± 0.17
		A. calcarea	24	1890	106.65	1.01	0.84 ± 0.12
Sta María	Vertical	*A. radiosa*	19	1889	52.61	0.41	0.36 ± 0.07
		A. calcarea	22	1897	62.67	0.51	0.48 ± 0.02
Sta Eugenia	Horizontal	*A. radiosa*	15	1904	51.34	0.38	0.26 ± 0.08
		A. calcarea	16	1853	59.87	0.53	0.35 ± 0.16
Sta Eugenia	Vertical	*A. radiosa*	6	1853	25.94	0.16	0.14 ± 0.02
		A. calcarea	14	1900	42.61	0.44	0.30 ± 0.11
Sencelles	Horizontal	*A. radiosa*	16	1897	101,17	0.40	0.26 ± 0.04
		A. calcarea	9	1855	86.79	0.84	0.34 ± 0.25
Sencelles	Vertical	*A. radiosa*	17	1882	42.17	0.27	0.19 ± 0.06
		A. calcarea	12	1897	38.00	0.42	0.23 ± 0.10

[1] Total 180 measurements. Note that the maximum lichen size measured in each cemetery does not have to correspond to the oldest grave.

Although in some lichen populations power and second-order polynomial functions displayed slightly better correlation ratios, we decided to select the linear regressions to achieve homogeneity of the results (Figure 10). The obtained functions were used to calculate the exposure age for the different lichen ribbons of the bedrock fault scarp, resulting in similar and coherent dates in the two analyzed species (Tables 2 and 3). Eventually, we calculated a mean regression equation for the populations of *A. radiosa* in the two cemeteries, since it was the lichen species with a better fit to the measurements taken in the fault scarp (Figure 11). The application of the obtained linear function for vertical populations of *A. radiosa* to the fault scarp ribbons resulted in average dates of 1950 ± 16.7 CE for the basal ribbon B1, 1852 ± 40.3 CE for ribbon B2 and 1773 ± 80.5 CE for the upper ribbon B3 (*Age 2:* Table 2).

The obtained functions for *A. calcarea* resulted in similar dates of 1966 ± 15.4 CE for the basal ribbon B1, 1849 ± 56.2 CE for ribbon B2 and 1763 ± 79.7 CE for the upper ribbon B3 (*Age 2:* Table 3). The calculation of direct numerical ages provides similar average dates using both species (*Age 1:* Tables 2 and 3). These results clearly indicate that the exposure date of the second ribbon (B2) lies within the range (1841–1855 CE) of the 1851 CE Palma earthquake [20,36]. Consequently, this second fault ribbon can be considered as a coseismic feature, but its characterization as a primary or secondary faulting feature is discussed in the following sections. Curiously, the average ages of the upper ribbon (B3) lie within the

range age of the first strong seismic event cataloged on the island, i.e., the VII EMS Selva event that occurred in 1721 CE near the locality of Selva (Figure 1) [36].

Table 2. Measurements of Aspicilia radiosa in the bedrock fault scarp. Age 1 corresponds to the direct application of the obtained mean growth rates for vertical populations in the Sencelles and Sta. cemeteries Eugenia (0.19 mm/yr). Age 2 corresponds to the average date (calendar age) resulting from the application of the obtained mean LGR liner regression function ($y = -4.829x + 2007$) shown in Figure 10. Average years and uncertainty (standard deviation) are shown for each analyzed ribbon (B1, B2, B3).

| Site	*Thallus* nº	Lichen Sp.	Ribbon	Size (mm)	Age 1 (Year)	Age 2 (Year)
FENCE	8	*A. radiosa*	B1	18.09	1979	1938
HOUSE	21	*A. radiosa*	B1	13.48	1948	1962
HOUSE	23	*A. radiosa*	B1	15.37	1937	1952
Average date					**1952 ± 17.1**	**1950 ± 16.7**
HOUSE	27	*A. radiosa*	B2	23.45	1888	1894
FENCE	29	*A. radiosa*	B2	24.07	1884	1891
HOUSE	32	*A. radiosa*	B2	28.74	1860	1868
HOUSE	26	*A. radiosa*	B2	32.66	1839	1849
HOUSE	30	*A. radiosa*	B2	48.29	1757	1774
FENCE	28	*A. radiosa*	B2	32.90	1838	1848
HOUSE	31	*A. radiosa*	B2	34.71	1828	1839
Average date					**1846 ± 44.1**	**1852 ± 40.3**
FENCE	45	*A. radiosa*	B 3	45.64	1771	1787
FENCE	46	*A. radiosa*	B3	48.65	1755	1787
FENCE	47	*A. radiosa*	B3	51.14	1742	1760
Average date					**1756 ± 14.5**	**1773 ± 80.5**
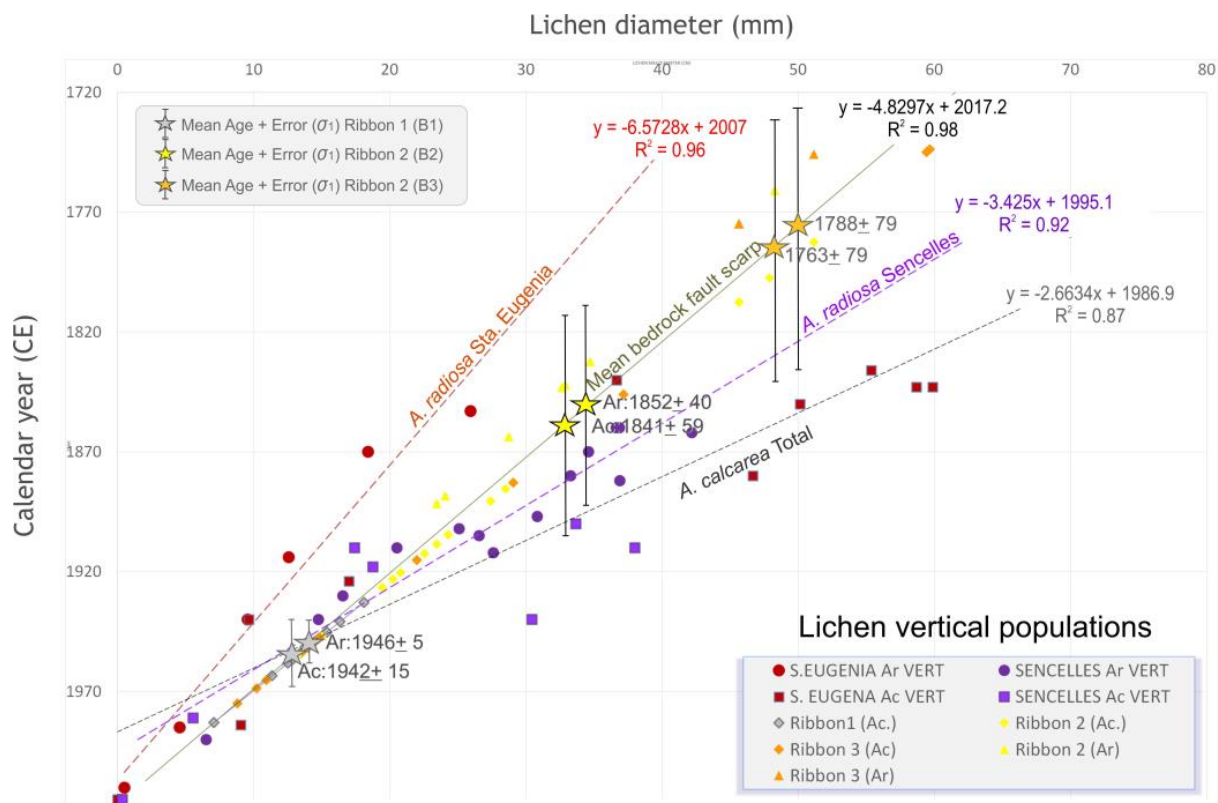
Figure 11. XY dispersion graphic showing the best-fit linear regression lines and corresponding equation for the vertical populations of lichens in the cemeteries of Sta. Eugenia and Sencelles located on the fault trace.

Table 3. Measurements of Aspicilia calacarea in the bedrock fault scarp. Age 1 corresponds to the direct application of the obtained mean growth rates for vertical populations in the Sencelles and Sta. Eugenia Cemeteries (0.22 mm/yr). Age 2 corresponds to the average date (calendar age) resulting from the application of the obtained mean LGR linear regression function (y = −4.829x + 2007) shown in Figure 10. Average years and uncertainty (standard deviation) are shown for each analyzed ribbon (B1, B2, B3).

Site	*Thallus* n°	Lichen Sp.	Ribbon	Size (mm)	Age 1 (Year)	Age 2 (Year)
HOUSE	4	*A. calcarea*	B1	7.07	1979	1997
HOUSE	15	*A. calcarea*	B1	11.36	1959	1976
HOUSE	5	*A. calcarea*	B1	12.51	1954	1971
HOUSE	3	*A. calcarea*	B1	12.87	1953	1969
HOUSE	2	*A. calcarea*	B1	13.97	1945	1964
HOUSE	1	*A. calcarea*	B1	14.49	1941	1961
FENCE	8	*A. calcarea*	B1	16.34	1929	1957
Average date					**1949 ± 9.9**	**1966 ± 15.4**
FENCE	14	*A. calcarea*	B2	13.38	1950	1962
HOUSE	16	*A. calcarea*	B2	13.57	1949	1962
HOUSE	12	*A. calcarea*	B2	15.00	1943	1954
HOUSE	13	*A. calcarea*	B2	19.46	1923	1931
HOUSE	11	*A. calcarea*	B2	20.23	1919	1927
FENCE	33	*A. calcarea*	B2	20.80	1916	1924
FENCE	34	*A. calcarea*	B2	22.55	1909	1916
FENCE	35	*A. calcarea*	B2	23.44	1904	1911
HOUSE	10	*A. calcarea*	B2	24.28	1901	1907
HOUSE	9	*A. calcarea*	B2	27.38	1887	1891
FENCE	36	*A. calcarea*	B2	27.40	1886	1891
HOUSE	17	*A. calcarea*	B2	28.50	1881	1885
HOUSE	24	*A. calcarea*	B2	45.64	1804	1797
HOUSE	25	*A. calcarea*	B2	45.65	1804	1797
HOUSE	22	*A. calcarea*	B2	47.88	1793	1786
HOUSE	20	*A. calcarea*	B2	51.14	1779	1769
Average date					**1855 ± 52.7**	**1841 ± 56.0**
HOUSE	7	*A. calcarea*	B3	8.80	1971	1986
FENCE	38	*A. calcarea*	B3	10.21	1965	1979
HOUSE	19	*A. calcarea*	B3	10.94	1961	1975
FENCE	37	*A. calcarea*	B3	13.61	1949	1961
HOUSE	10	*A. calcarea*	B3	13.96	1948	1960
HOUSE	18	*A. calcarea*	B3	14.46	1945	1957
FENCE	40	*A. calcarea*	B3	14.84	1944	1955
FENCE	41	*A. calcarea*	B3	14.98	1911	1954
HOUSE	6	*A. calcarea*	B3	21.97	1879	1918
FENCE	42	*A. calcarea*	B3	37.17	1842	1841
FENCE	43	*A. calcarea*	B3	59.43	1741	1727
FENCE	44	*A. calcarea*	B3	59.66	1740	1725
Average date					**1781 ± 75.2**	**1763 ± 79.9**

6. Fault Trench Analyses at the Base of the Scarp

A small fault trench was excavated in 2002, adjacent to the fault-scarp, after detailed geomorphological, geophysical, and topographic (5 cm/pixel DEM) analysis of the Sta. Eugenia fault segment [20,35]. The trench was dug with a backhoe excavator perpendicular to the fault scarp, with a N150° E orientation. Due to the absence of datable material, the trenching results were only preliminarily reported in a post-conference field trip of the Sixth International Congress of the International Union of Geomorphology (IAG) held in Spain in 2005 [23]. So, it is in this work that the fault trench of the SCF is fully described. The purpose was to compare and relate, if possible, the different identified lichen ribbons with probable exposure events of the fault plane recorded as colluvial wedges within the trench.

The trench was 16 m long, 4 m wide and 3.5 m deep, and it was excavated only in the softer sedimentary filling of the hanging wall of the fault (Figure 12). The SW limit of the

trench was constituted by the subvertical scarp generated by the bedrock fault plane itself. The last 15 cm adjacent to the fault plane were excavated and cleaned by hand to preserve the kinematics features of the fault zone. This fault zone displayed a narrow fault breccia with a thickness between 14 and 46 cm, widening upwards with anastomosing fault planes and positive-flower structure, fitting the geometry of a strike-slip fault [37]. The breccia was intensely sheared and crushed incorporating deformed fragments of calcarenites, breached fragments of *Ostrea* sp., and detached subvertical mud clasts of some of the Quaternary deposits adjacent to the fault plane.
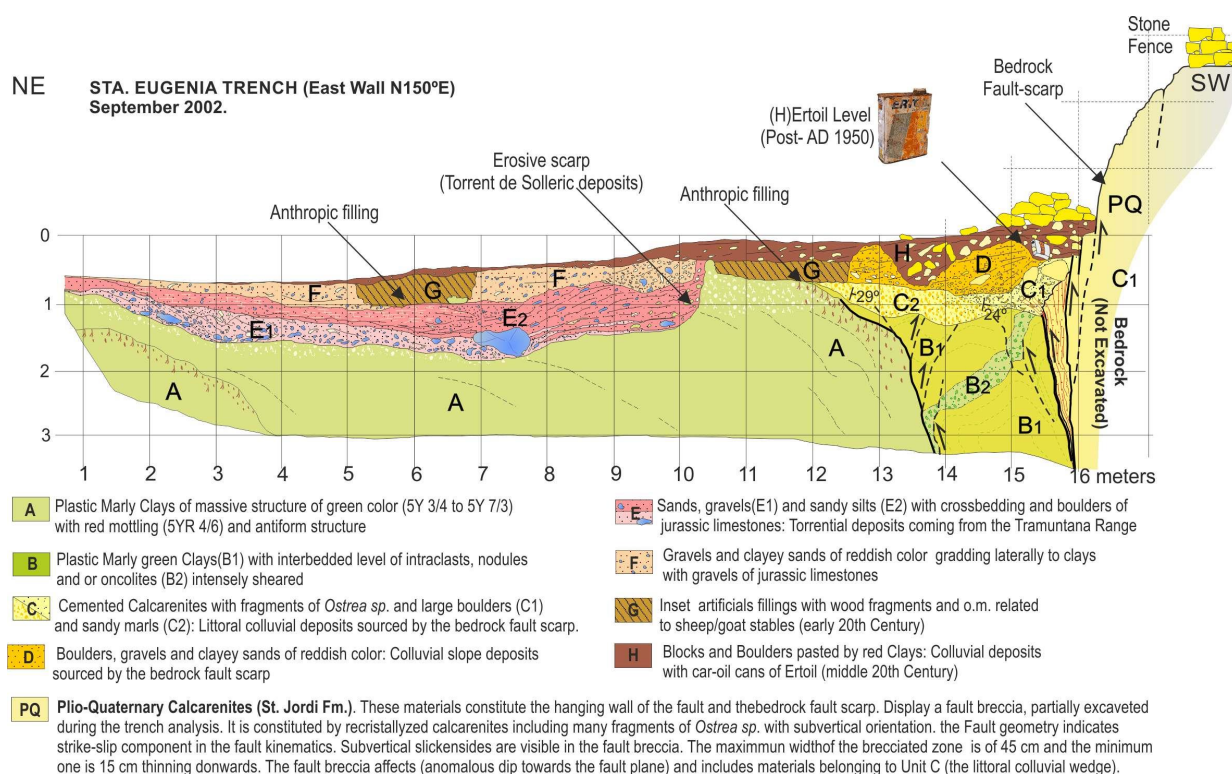

Figure 12. Log of the eastern wall of the trench excavated east of the cemetery of Sta. Eugenia (39°37.541′ N; 2°50.943′ E) in the year 2002. See the text for an explanation.

The footwall of the fault is entirely constituted by Plio-Quaternary calcarenites of the St. Jordi Fm. (see Figure 2), composed of recrystallized coarse-grained calcarenites with an important amount of *Ostrea* sp. and other bivalve molluscs or scallops (*pectinidae*) occasionally generating shelly levels (lumachella facies). These materials are considered of littoral origin, with shore facies and even aeolian sediments in their upper sequences [17,18]. On the contrary, the hanging wall is mainly constituted by deformed massive greenish-grey clayey marls (5Y 3/4 to 5Y 7/3) affected by diffuse gley mottling (10YR 6/6), with minoritarian clastic deposits. They constitute a massive plastic body with several sedimentary markers (i.e., apparent paleosols with small rhizoconcretions, carbonate nodules and mottling horizons) delineating an overall anticline subparallel to the fault (Unit A; Figure 12). Several fissures and slickenside planes between meters 10 and 14 of the log display convex geometries of a general N55-65° E strike and maximum dip of 65° SW, delineating the southern limb of the antiform. This limb is intensely deformed close to the fault plane, forming a subvertical 65–78° SW dipping sheared body, about 2 m thick between meters 14 and 16 of the log adjacent to the fault plane (Unit B1; Figure 12). This unit represents the zone of principal displacement (ZPD) of the fault zone and consists of intensely sheared and folded massive dark green (5Y 7/3) plastic clays forming a sheared vertical body. It can be considered as an incohesive clayey fault gouge featured by upwards branching synthetic and antithetic reverse slickenside planes. Its internal deformation is

highlighted by a strongly distorted level formed by nodules of indurated marls and/or oncoids (Unit B2). The nodules have a mean 10–30 mm diameter with a maximum size of 45 mm, displaying subrounded to elliptical geometries, the last being subvertically elongated along the strata dip. This intraclastic level showed severe distortion, displaying an asymmetric folding and shearing in the intersection points of meters 3/13 and 2/14 of the grid (Figure 12).

The northern limb of this fold was eroded by a sharp 1.4 m high scarp carved in the clayey marls overlapped by cross-bedding torrential deposits without any apparent deformation (Units E and F). The bases of these torrential deposits contained coarse gravels and large boulders of Jurassic limestone coming from the Tramuntana Range (Unit E1) pasted in a reddish-orange sandy-clayey matrix (2.5 YR 4/6). Jurassic gravels were also frequent in the overlying units E2, and F (Figure 12). Unit E2 presented a strong recarbonation and cementation, suggesting a long period of no-sedimentation before the deposition of the following unit. Unit F had smaller gravels embedded in a fine-grained sandy-clayey matrix of reddish color like that of Unit E1. Both units presented scattered angular gravels of the calcarenitic bedrock of the fault as well as large mud clasts of the underlying clayey marls, but only near the scarp channel or in the basal channel lag facies (Figure 12). The fluvial deposits are certainly of the Late Quaternary age (presumably Holocene) and related to the Torrent de Solleríc (see Figure 3), which runs parallel to the Sencelles fault around the excavated zone [19,20].

The age of the clayey marls of units A and B is unclear. The occurrence of rizhoconcretions, carbonate nodules, and gley mottling suggests a subaerial or intertidal origin. The lack of datable material along the entire excavated trench impeded any chronological assignation for these units. However, it could correspond to the *Bonanova Fm.*, the *Santanty Fm.* (marls and calcisiltites), or some other member of the so-called Fini-Messinian Terminal Complex (see cross-section of Figure 2). These formations display mangrove to lagomare tidal facies in this sector of the Inca basin, and according to the borehole and geophysical data [17,18,38], they are close to the surface. In fact, detailed Very Low-Frequency electromagnetic profiles (VLF) carried out before the excavation of the trench detected a subsurface diapiric-like body in the hanging wall of the fault [20,35]. This suspect clayey diaper is rooted at 60 m depth and its upper figure match-well with the deformation shown in the clayey antiform of Unit A (see Figure 8 Silva et al., 2001 [20]; p. 257).

Three different colluvial units sourced by the fault scarp occurred only adjacent to the bedrock fault scarp in the fault trough (2.6 m width) generated by the flanking anticline. These colluvial units overlapped (Units C, D, H), burying the last 0.95 m of the excavated fault plane between meters 15 and 16 of the log (Figure 12). Finally, the upper 2.05–2.45 m remained exposed as the free face of the bedrock fault scarp. The colluvial Unit C is constituted by sandy marls (C1) grading laterally to yellow calcarenites (Unit C2), which include broken fragments, clasts, and large boulders (60 × 40 cm) of the fault bedrock. Its matrix is a strongly cemented (recrystallized) coarse-medium-grained calcarenite, that includes numerous broken fragments of *Ostrea* sp., coming from the bedrock. The sandy marls (Unit C1) presented a massive assemblage and are affected by an intense re-carbonation with many nodules of carbonate. The whole unit displayed a yellowish color (2.5Y7/6–8) and did not incorporate weathered material (i.e., terra rossa) from the calcarenitic substratum. Unit C can be interpreted as a littoral colluvial wedge (C2) grading laterally to a narrow littoral sag-pond (C1) that is accommodated within the trough generated along the fault zone above Unit B1. The anomalous dip of the base of C1 towards the fault plane, near its contact with the antiform of unit A (meter 12 to 14 in the log) suggests that these littoral deposits have been slightly tilted due to the growth of the clayey bulge of unit A. Unit C constitutes the last evidence of littoral sedimentation along the fault zone, probably during the Lower Pleistocene, but the first evidence of probable surface faulting during the Quaternary within the excavated trench. The absence of weathered material in unit C suggests that it was formed soon after the sedimentation of littoral calcarenites (beach and dune sediments) in this zone. On the other hand, the

intense secondary recarbonation affecting Unit C indicates a relatively long period of neither sedimentation nor fault activity until the deposition of the overlying Unit D.

The colluvial Unit D contains angular and weathered clasts and boulders of the Pliocene bedrock (Unit PQ), pasted by a reddish sandy-clay matrix (2.5YR 5/6) also including reworked and broken fragments of *Ostrea* sp. Unlike unit C, unit D is weakly cemented and easily removed by pick. Adjacent to the fault (meters 12 to 16; Figure 12) there are some clast-supported subangular boulders and gravels, these last with sizes ranging from 2 to 5 cm in diameter. These alluvial deposits are clearly sourced by the upthrown block of the fault and can be considered as a colluvial wedge related to Pleistocene to Holocene fault activity. However, this colluvial wedge did not display evidence of faulting. Data from both walls of the excavated trench indicate that this colluvial wedge does not extend beyond meter 12 to the north, seeming to shift laterally into the deposits of unit F, which displays a similar clast composition and reddish coloring. However, clasts in Unit F are smaller (<2 cm), very sparse, and matrix-supported, incorporating small gravels of the calcarenitic bedrock (Figure 12), which allows us to infer that they are the distal part of Unit D merging with the alluvial deposits sourced by the Torrent de Solleríc. In fact, the combined top surface of units D+F constituted a former ground surface, which is disturbed and affected by ancient artificial pits and trenches related to sheep and goat livestock farming during the first half of the 20th century (Units G and H; Figures 12 and 13). Where observed, the past ground surface D+F did not display soil signals, which together with the loose cementation of their materials allows us to infer a very recent age for it.
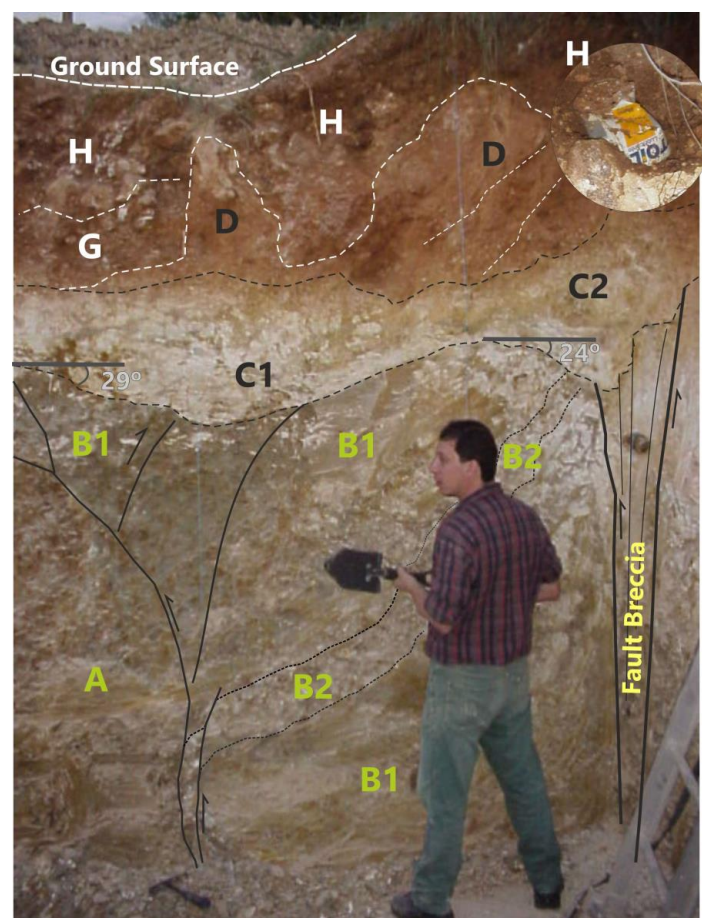

Figure 13. Photo of the fault zone in the eastern wall of the excavated trench highlighting the position and location of the different units and structures displayed in Figure 11. Green letters: Plastic clayey units; Black letters: Colluvial wedges; White letters: artificial fillings. The middle-20th-century Ertoil level (Unit H) is magnified.

Eventually, the disturbed D+F surface is entirely buried by a third colluvial unit of anthropogenic origin (man-made). This unit (H) is constituted by reddish-brown clays (2.5 YR 4/6–8) with angular and rectangular blocks of calcarenites (30 × 20 cm) coming from a ruined stone fence located on top of the fault scarp, but also by some weathered blocks of the underlying unit D (Figures 12 and 13). This unit fills the man-made pits carved on the surface of unit D and it contains post-1950 CE car-oil cans of Ertoil trademark (Figures 12 and 13), which places the formation of this artificial unit in the second half of the 20th century. Consequently, this man-made rubble unit postdates the 1851 earthquake and the artificial fillings of unit G. Besides the colluvial wedges C and D, no earthquake evidence can be deduced from the excavated trench. These two overlapped colluvial wedges may indicate repeated fault scarp reactivations during the Quaternary, but of unknown age.

7. Discussion

The lichenometric analysis developed in this paper indicates a high sensitivity of LGR to the position (vertical/horizontal) and geographical orientation of the exposed rocky surfaces. This occurs at short distances (6 km maximum), and even in the same location, a cemetery in our case (Figures 9 and 10). As it was expected, horizontal populations of lichens display larger LGR, than the vertical ones, but these last are the most suitable ones for the chronological analysis of the vertical bedrock scarp of the Sencelles Fault. Among the differently oriented vertical lichen populations, those facing the NW, like the bedrock fault scarp, resulted in the most appropriate for this study (Figure 12).

Eventually, only the vertical populations (facing NW) of the cemeteries of Sta. Eugenia and Sencelles, located on the fault trace (Figure 2), were used to calculate the LGR of the two lichen species used in this study (Figure 12). In both cases, mean growth rates for *A. calcarea* (0.22–0.23 mm/yr) were always higher than those for *A. radiosa* (0.16–0.19 mm/yr) (Figure 11; Table 1). Mean LGR for the vertical datasets of *A. calcarea* and *A. radiosa* indicated that the differentially colonized ribbons of the basal fresh scarp (Figure 8) have a historical age as old as the early 16th century (Tables 2 and 3). On the contrary, the upper rugged section of the scarp was largely colonized by black lichen colonies overlapped by the orange crustose lichen *X. calcicola* and by large coalescent colonies of *A. calcarea* unsuitable for lichenomrretric analysis. As indicated by the survival time of lichen colonization in limestone surfaces before flaking at 700–800 years [7,31], this upper segment of the scarp may have an age predating the 12th century. However, considering its weathering stage (solution pits), scarp retreat (78 cm), and scarp angle (45–75°), this scarp segment should have a Holocene age probably older than 3500 years before the present (Figure 8).

As mentioned in Section 5, the obtained ages for the older ribbon (B3) of the basal historical scarp are near the range of the first strong earthquake documented on the island: the 1721 CE earthquake (VII EMS–VIII ESI07) near the locality of Selva [36], 12 km north of the fault scarp (Figure 1). This is a doubtful seismic event, recently characterized as a giant mass-movement event by some authors (Biniarroi complex landslide) [39]. This large avalanche affected an area of 296,000 m^2 and mobilized more than 2 million cubic meters of poorly consolidated Plio-Quaternary materials, generating a high variety of ground failures and hydrogeological changes [39]. The event affected several houses in the small village of Biniarroi and it was felt at Selva as a large tremor [23–25]. In the case of a coseismic landslide, their huge dimensions will indicate a minimum local intensity of VIII ESI07 [40]. Whatever the case, this event is still cataloged as an intensity VII EMS earthquake in the official seismic databases of Spain [36]. These same catalogs list other smaller earthquakes (IV–V EMS) in the environs of Sta. María del Camí and Sencelles between the years 1763 and 1773 CE (Figure 1), also within the range of the computed age for ribbon B3 (Figures 8 and 10). These two last historical events have their macroseismic epicenters near the locality of Sencelles (Figure 1) and they can be related to the activity of the SCF but not to any of the studied ribbons or trench units. However, the dimensions of the third ribbon of the scarp B3 (c. 70 cm) preclude its correlation with any of the mentioned

events, suggesting instead a prehistorical age for the causal event. The colluvial wedge of Unit C is the oldest one (Figure 12). This unit is free of *terra-rossa*, strongly cemented, and displays littoral features impossible to corelate with the obtained lichenometric ages (c. 1700 CE) of the basal fresh fault plane (Tables 2 and 3). The absence of weathered materials suggests that this unit must be close in age to the end of the sedimentation of the Plio-Pleistocene littoral calcarenites of the St. Jordi Fm [18–20], that is, an early Pleistocene age probably at the end of the Gelasian Stage (ca. 2.0–1.8 Ma) related to the latest coastal environments in the central sector of the island. Consequently, this unit could be related, in the best of cases, to the uppermost vegetated part of the rugged band of the scarp, testifying to the early activity of the fault during the Quaternary Period.

The ages computed for the second ribbon of the scarp (B2) lay within the time range of the 1851 CE earthquake (VII EMS), between ca. 1840 and 1855 CE (Tables 2 and 3). Therefore, this ribbon could be tentatively related to the modern colluvial wedge of the fault trench (Unit D), which may constitute the youngest natural colluvial slope of the fault scarp (Figure 12). This unit contains an important amount of *terra-rossa* in its reddish clayey matrix which indicates a long exposure time of the footwall after the deposition of the underlying Unit C. In this case, the colluvial deposits of Unit D may be related to the second ribbon of the scarp (B2). Finally, the basal fault scarp ribbon (B1) is modern in age, and it can be assigned to the middle 20th century (ca. 1950–1960 CE; Tables 2 and 3). This age fits well with the age of the upper colluvial deposits containing oil-car cans (Unit H; Ertoil level) documented in the fault trench (Figures 12 and 13). The exposure of this thin ribbon can be related to the excavation works carried out in the zone during the middle 20th century for ground leveling and preparation for the agricultural development of the area. Probably, these works also included the trimming of shrubbery along the complete scarp. In fact, there is an important population of lichen sizes of this age in all ribbons (Tables 2 and 3), possibly favored by better exposure after the removal of vegetation along the scarp.

Despite the absence of an unequivocal relationship between the second ribbon (B2) and the colluvial wedge of unit D, this last constituted the colluvial slope adjacent to the fault scarp before the excavations work and artificial fillings related to units G and H (Figure 12) were carried out. In this way, the lichenometric age obtained for the B2 ribbon allows to link this colluvial ground surface with the landform assemblage around the fault scarp during, or soon after, the 1851 CE earthquake. In spite of the activity of the SCF during Neogene and Quaternary times [17–22], the studied lichen ribbons cannot be considered surface faulting features. The dimensions of the ribbons (40–70 cm average width) along the whole length of the Sta. Eugenia fault segment (840 m) rule out these ribbons as primary faulting features [40]. In detail, the small size of ribbon B2 (23–47 cm wide) set aside this feature from the minimum dimensions required for surface faulting after the more basic empirical relationships between earthquake magnitude, average displacement, and surface rupture length [41]. However, the obtained lichen chronology allows us to consider the studied lichen banding as coseismic features, but of secondary origin, and in particular ribbon B2 to the 1851 CE earthquake. In this case, a maximum displacement of 0.47 m (maximum width of ribbon B2) for the responsible exposure event might be assumed (Figures 4 and 8), being classified as coseismic ground failure along the pre-existing fault scarp [42].

Regarding the secondary coseismic origin of fault banding features, historical reports describe the occurrence of "generic" ground failure cases in the macroseismic area (Sa Cabaneta, to Sta. Eugenia; Figure 3) during the main earthquake (VII EMS) and the stronger aftershock (VI EMS) [24–26]. Modern surveys identified the occurrence of sympathetic faulting and coseismic subsidence at the Portol Doline (Figure 3) attributing them to the 1851 CE historical earthquake [20,43]. In this sense, the scarp ribbon B2 can be considered a coseismic sympathetic rupture [11] along the SCF trace or a secondary ground failure cataloged in the ESI07 Macroseismic Scale (i.e., gravity-assisted ground cracking) [40]. Macroseismic analyses based on the ESI07 scale indicate that this earthquake reached intensity VIII between Sa Cabaneta and Sta. Eugenia, a minimum intensity of VII in Palma

City and Palma Bay and an intensity of VI in the studied zone (Figure 1), resulting in a maximum magnitude of 4.6–4.8 Mw [44].

Additionally, the main earthquake and stronger aftershocks caused significant archaeoseismic damage in the cathedral and most of the churches of Palma City as well as the destruction of the St. Marçal Church in Sa Cabaneta [24–26], 3 km away from the studied zone (Figs 1 and 3). In this sense, some of the oldest funerary monuments in the cemetery of Sta. Eugenia show suspected evidence of earthquake damage. This is the case of the mausoleum of "Juan Castell y Los Suyos", dated in 1853 CE (Figure 7d), but very probably built soon before the 1851 CE earthquake during the early construction of this cemetery around 1843 CE [29,30] (see Section 3). The mausoleum displays typical elements of archaeoseismic damage [45], such as the dropped keystone, penetrative fractures, and broken dipping corners on the doorway lintel. These earthquake archeoseismic effects only develop from intensity VI–VII [44] and they cannot be attributed to seismic events in the zone that occurred after 1851 CE, all of them with intensities $\leq$ IV [36].

8. Conclusions

The lichenometric analysis of the bedrock fault scarp of the Sta. Eugenia segment of the SCF (Mallorca Island) revealed the occurrence of different exposure events of the fault plane evidenced by differential lichen colonization. These recurrent exposure events result in a clear fault banding that differentiates a lower subvertical fresh fault plane (1.29 m) from an upper and older weathered and karstified one (1.16 m) of rugged topography. These two bands displayed different colonization degrees by two lichen species typical of calcareous rocks: *Aspicilia calcarea (Ac) and Aspicilia radiosa (Ar)*, which could identify up to six ribbons differentially colonized by these lichens. Lichen growth rates (LGR) regression equations have been constructed from lichen growth data collected in three cemeteries of the zone, two of them located onto the studied trace of the SCF. After a systematic statistical analysis of differentially oriented lichen populations (DOLPs), we selected the vertical populations oriented to the NW by their analogy with the studied rocky fault scarp.

The lichenometric analysis indicated that the lower band of the fault scarp (ribbons B1 to B3) have historical ages from before the 16th century. In detail, the ages obtained for ribbon B2 (ca. 1840–1855 CE) allow us to relate it with the 1851 CE Palma Earthquake (VII EMS–VIII ESI07). The dimensions of ribbon B2 (max. 0.47 m width) when compared with its short length along the Sta. Eugenian segment (840 m) rule out its classification as a surface-faulting feature [40,41] but as some kind of secondary or sympathetic rupture along the fault trace. As defined by Serva [11,42] a sympathetic rupture is a displacement triggered along a fault that is completely isolated from the main seismogenic fault. The coseismic displacement is due to gravity effects along the fault plane triggered by local stress changes induced by seismic wave propagation, which can occur even far away of the seismogenic fault [11]. This kind of gravity ground failure can also occur during coseismic ground shacking and cracking especially in vertical contacts separating differentially compacted geological materials [40], and particularly in bedrock faults. The application of the ESI07 scale to this feature (ribbon B2) implies a maximum intensity of VIII for the event. Since we are on the trace of a fault active during Neogene and Quaternary times [17–20], the older analyzed ribbons (B3 to B6; Figure 8) can be assumed to be related to similar coseismic mechanisms caused by older exposure events. The obtained lichen ages indicate that ribbon (B3) can be related to the suspect earthquake (VII EMS) that occurred on the island in 1721 CE, but this event has been recently featured as a huge landslide occurred in the Tramuntana Range [39] about 15 km away from the SCF (Figure 1). The two last ribbons featuring the upper c. 150 cm (B5 and B6) of the fault scarp display evident signals of differential weathering and karstification (Figure 8). These may represent more ancient Holocene earthquakes, presumably within the range of the last 3000–4500 years. Preliminary lichen observations on prehistoric Talayots (1200–1500 BCE) in the island indicate that they display similar lichen assemblages and populations than those observed in the upper ribbons of the ancient fault scarp. However other causes such as fault plane

exhumation by erosion processes cannot be ruled out, and maybe these upper older ribbons (B5 and B6) may represent a difficult-to-assess mixture of exhumation by tectonic and non-tectonic processes. Eventually, the basal ribbon B1 can be linked to ground leveling works carried out during the middle 20th century, which matches with the data coming from the trench excavated in the zone in the year 2002 (Figure 11). This ribbon can be linked to the upper colluvial deposits documented in the trench containing oil-car cans.

Data from fault trenching did not throw any geochronological data, but present colluvial deposits clearly sourced by the studied bedrock fault scarp (units C and D; Figure 11). Among these units, only unit D (not dated) can be labeled as a clear colluvial wedge and it might be theoretically related to the landform assemblage around the fault scarp soon before or during the 1851 CE earthquake. However, deformation structures documented in the trench (antiform; slickensides surfaces, sheared vertical clayey body adjacent to the fault plane) point to a strike-slip kinematics subsidiary to the normal behavior usually assigned to the SCF [21]. The combined data of lichenometry, fault trenching, and the length of the analyzed fault scarp (c. 840 m) indicate that the studied segment of the fault cannot be considered a co-seismic surface faulting related to the 1851 CE event, but a relevant secondary earthquake effect on a pre-existing fault scarp (sympathetic ground ruptures). No-surface faulting events occur in the Sencelles fault able to cause the observed displacements (lichen ribbons), but sympathetic displacements triggered by relatively distant earthquakes seem to be the most probable causative events. In the case of the 1851 CE earthquake, sympathetic ruptures are the better fitting solution, since other normal faults of the island (i.e., Cap Enderrocat Fault; Figure 1) have been proposed as the seismogenic source of that event [46].

The systematic lichenometric analysis performed in this work constitutes the first attempt to date a bedrock fault scarp by means of lichen analyses. Most of the published lichen analyses [1–8] only consider the dating of horizontal rocky surfaces, where lichen growth rates are higher, but this work evidences that vertical surfaces can also be easily dated by this method. The method represents a low-cost alternative to the most expensive methods based on cosmogenic isotopes [14,15,32,33]. However, complementary age controls are recommended, whether these are isotopic, morphometric, or coming from fault trenching analyses. Lichenometry can thus be used as a first primary step to plan further dating techniques. Although positive relationships between surface lichen colonization, roughness, and surface age are expected to occur in recurrent exposure events in a bedrock fault scarp, lichenometry alone cannot be used to assess the coseismic, tectonic, or non-tectonic nature of exposure events related to fault banding. The selection of an area with close monuments and cemeteries accessible for lichen analyses is the best option, always considering the geographical orientation of the analyzed rocky surfaces. As indicated in this study, lichen growth rates are very sensitive to geographical orientation and lithology, so general or regional LGR functions must be applied with caution, and it is preferable to construct local LGR functions with data from around the studied zone.

Author Contributions: Project design, management, conceptualization, coordination, funding acquisition, fieldwork, fault trenching analyses, design of graphic information and writing—original draft preparation, P.G.S.; fieldwork, field sampling, and writing—review and editing, E.R.; fieldwork, geochronological analysis, management of geochronological data, design of graphic information and writing—review and editing, R.P.-L.; fieldwork, field sampling geochronological data, writing—review and editing, T.B.; fieldwork, fault trenching analyses, graphic information G.S.D.; design of graphic information and GIS management, J.E. All authors have read and agreed to the published version of the manuscript.

Institutional Review Board Statement: Not applicable.

Informed Consent Statement: Not applicable.

References

1. Innes, J.L. The use of lichens in dating. In *Handbook of Lichenology*; Galun, M., Ed.; CRC Press: Boca Raton, FL, USA, 1988; Volume III, pp. 75–91.
2. Benedict, J.B. Experiments on Lichen Growth, III. The Shape of the Age-Size Curve. *Arct. Antarct. Alp. Res.* **2008**, *40*, 15–26. [CrossRef]
3. Bull, W.B. Lichenometry dating of coseismic changes to a New Zealand landslide complex. *Ann. Geophys.* **2003**, *46*, 1155–1167.
4. Bull, W.B. Dating San Andreas Fault earthquakes with lichenometry. *Geology* **1996**, *24*, 111–114. [CrossRef]
5. Pérez-López, R.; Giner-Robles, J.L.; Rodríguez-Pascua, M.A.; Silva, P.G.; Roquero, E.; Bardají, T.E. Lichenometric dating of coseismic rockfall related to the Great Lisbon Earthquake in 1755 affecting the archaeological site of "Tolmo de Minateda" (Spain). *Z. Für Geomorphol.* **2019**, *62*, 271–293. [CrossRef]
6. Jomelli, V.; Grancher, D.; Naveau, P.; Cooley, D.; Brunstein, D. Assessment study of lichenometric methods for dating surfaces. *Geomorphology* **2007**, *86*, 131–143. [CrossRef]
7. Pérez-López, R. Datación por liquenometría aplicada en geomorfología, clima y arqueología. *Cuatern. Y Geomorfol.* **2022**, *36*, 11–23. [CrossRef]
8. Wallace, R.E. Profiles and ages of young fault scarps, north-central Nevada. *Geol. Soc. Am. Bull.* **1977**, *88*, 1267–1281. [CrossRef]
9. Wallace, R.E. Fault scarps formed during the earthquake of October 2, 1951, in Pleasant Valley, Nevada, and some tectonic implications. *USGS Prof. Pap.* **1984**, *1274*, 1–33.
10. Silva, P.G.; Roquero, E.; Bardají, T.; Pérez-López, R.; Rodríguez-Pascua, M.A.; Giner-Robles, J.L.; Perucha, M.A. Geochronology of the Sencelles fault scarp and its relationships with the AD 1851 Mallorca Earthquake (Baleares Islands, Spain). *Geo-Temas* **2016**, *16*, 653–656.
11. Serva, L. Ground effects in intensity scales. *Terra Nova* **1994**, *6*, 414–416. [CrossRef]
12. dePolo, C.M.; Clark, D.G.; Slemons, B.; Ramelli, A.R. Historical surface faulting in the Basin and Range province, western North America: Implications for fault segmentation. *J. Struct. Geol.* **1991**, *13*, 123–136. [CrossRef]
13. Pérez-López, R.; Rodríguez-Pascua, M.A.; Silva, P.G.; GinerRobles, J.L.; Bischoff, J.L.; Owen, L.A. Calibración de la curva de crecimiento para Aspicilia radiosa aplicada en dataciones liquenométricas. In *Reunión Nacional de Geomorfología*; Abstract; Solsona: Barcelona, Spain, 2010; Volume XI, pp. 503–507.
14. Schlagenhauf, A.; Gaudemer, Y.; Benedetti, L.; Manighetti, I.; Palumbo, L.; Schimmelpfennig, I.; Finkel, R.; Pou, K. Using in situ Chlorine-36 cosmonuclide to recover past earthquake histories on limestone normal fault scarps: A reappraisal of methodology and interpretations. *Geophys. J. Int.* **2010**, *182*, 36–72. [CrossRef]
15. Zoua, J.; Hea, H.; Yokoyamab, Y.; Shirahama, Y.; Sprosond, A.D.; Weia, Z.; Shia, F.; Haoa, H.; Miyairid, Y.; Lüe, L.; et al. Seismic history of a bedrock fault scarp using quantitative morphology together with multiple dating methods: A case study of the Luoyunshan piedmont fault, southwestern Shanxi Rift, China. *Tectonophyscis* **2020**, *788*, 228473. [CrossRef]
16. Acosta, J.; Canals, M.; López-Martínez, J.; Muñoz, A.; Herranz, P.; Urgeles, R.; Palomo, C.; Casamor, J.L. The Balearic Promontory geomorphology (western Mediterranean): Morphostructure and active processes. *Geomorphology* **2003**, *49*, 177–204. [CrossRef]
17. Capó, A.; García, C. Basin filling evolution of the central basins of Mallorca since the Pliocene. *Basin Res.* **2019**, *31*, 948–966. [CrossRef]
18. Benedicto, A.; Ramos, E.; Casas, A.; Sabat, E.; Barón, A. Evolución tecto-sedimentaria de la cubeta neógena de Inca (Mallorca). *Rev. Soc. Geológica España* **1993**, *6*, 167–176.
19. Sàbat, F.; Gelabert, B.; Rodríguez-Perea, A.; Giménez, J. Geological structure and evolution of Majorca: Implications for the origin of the Western Mediterranean. *Tectonophysics* **2011**, *510*, 217–238. [CrossRef]
20. Silva, P.G.; González Hernández, F.M.; Goy, J.L.; Zazo, C.; Carrasco, P. Paleoseismicity and historical seismicity in the Mallorca Island (Baleares, Spain): A preliminary approach. *Acta Geol. Hisp.* **2001**, *36*, 245–266. Available online: https://raco.cat/index.php/ActaGeologica/article/view/75647 (accessed on 1 December 2022).
21. Más, G.; Gelabert, B.; Fornós, J. Evidence of strike-slip displacement of the Sencelles fault (Mallorca, Balearic Islands). In *Reunión Ibérica Sobre Fallas Activas y Paleosismología, IBERFAULT II*; Abstract; Lorca: Murcia, Spain, 2014; Volume 2, pp. 47–50.
22. Giménez, J. Nuevos datos sobre la actividad post-Neógena en la Isla de Mallorca. *Geogaceta* **2003**, *33*, 79–82.
23. Silva, P.G.; Goy, J.L.; Zazo, C.; Giménez, J.; Fornós, J.; Cabero, A.; Bardají, T.; Mateos, R.; Hillaire-Marcel, C.; Bassam, G. Mallorca Island: Geomorphological evolution and neotectonics. Field-trip Guide Book (A7). In Proceedings of the 6th International Conference on Geomorphology, IAG-SEG, Zaragoza, Spain, 7–11 September 2005.
24. Pujó, M. Le tremblement de terre du 15 mai 1851 de l'île de Majorque. *Comp. Rend. Acad. Sci. Paris* **1851**, *2*, 23.

25. Bouvy, P. Sobre el Terremoto ocurrido en la Isla de Mallorca el 15 de mayo último. *Rev. Min.* **1851**, *2*, 375–378.

26. Bouvy, P. Notice sur le tremblement de terre du 15 mai 1851 de l'île de Majorque. *Bol. Soc. Géol. France* **1853**, *10*, 359–364.

27. Noller, J.; Locke, W.W. Liquenometry. In *Quaternary Geochronology*; Noller, J., Sowers, J.M., Lettis, W.R., Eds.; The American Geophysical Union: Washington, DC, USA, 2000; pp. 261–272. [CrossRef]

28. Lupiañez Fernández, D. Los cementerios de montaña en la Isla de Mallorca: Los casos de Deià, Establsiments y La Villeta. In *Resúmenes XX Encuentro de Cementerios Patrimoniales de España*; Red Española de Cementerios Patrimoniales: Málaga, Spain, 2019; pp. 1–13.

29. Peral Pacheco, D. El cólera y los cementerios en el siglo XIX. *Norba. Rev. Hist.* **1992**, *11*, 269–278.

30. Rodríguez Morín, F. El enterramiento en los cementerios, un asunto de salud prioritario para los liberales de Mallorca en 1812. *Estud. Hum. Hist.* **2015**, *14*, 99–124. [CrossRef]

31. Chen, J.; Blume, H.P.; Beyer, L. Weathering of rocks induced by lichen colonization—A review. *Catena* **2000**, *39*, 121–146. [CrossRef]

32. Mechernich, S.; Schneiderwind, S.; Mason, J.; Papanikolaou, I.D.; Deligiannakis, G.; Pallikarakis, A.; Binnie, S.A.; Dunai, T.J.; Reicherter, K. The seismic history of the Pisia fault (eastern Corinth rift, Greece) from fault plane weathering features and cosmogenic 36Cl dating. *J. Geophys. Res.* **2018**, *123*, 4266–4284. [CrossRef]

33. Zielke, O.; Benedetti, L.; Martin Maia, P.; Fleury, J.; Rizza, M.; Viseur, S. Bedrock fault roughness resolves slip increments of large earthquakes: Case studies from Central Italy. *Tectonophysics* **2022**, *838*, 229502. [CrossRef]

34. Rodríguez-Pascua, M.A.; Pérez-López, R.; Calvo, J.P.; García del Cura, M.A. Recent seismogenic fault activity in a Late Quaternary closed-lake graben basin (Albacete, SE Spain). *Geomorphology* **2008**, *102*, 169–178. [CrossRef]

35. Silva, P.G.; Carrasco, P.; González Hernández, F.M.; Goy, J.L.; Zazo, C.; Luque, L.; Santos, G.; Delgado, M.; Poza, L.J. Prospección Geofísica de la Falla de Sencellles (Mallorca, España): Una metodología preliminar para la realización de trincheras de falla. *Geotemas* **2000**, *1*, 360–363.

36. IGN On-Line Seismic Data Base. Most Important Earthquakes for Provinces in Spain. Consulted 22 February 2023. Available online: https://www.ign.es/web/ign/portal/terremotos-importantes (accessed on 1 December 2022).

37. Woodcock, N.H.; Fischer, M. Strike-slip duplexes. *J. Struct. Geol.* **1986**, *8*, 725–735. [CrossRef]

38. Morey, B. El registro Messiniense de la isla de Mallorca (archipiélago Balear, Mediterráneo occidental): Revisión e interpretación. *Estud. Geológicos* **2018**, *74*, e083. [CrossRef]

39. Giménez, J.; Mateos, R.M. Analysis of the Biniarroi (Mallorca) complex landslide. In Proceedings of the 4th EGS Plinius Conference on Mediterranean Storms, Maratea, Italy, 14–16 October 1999; Geophysical Research Abstracts. European Geophysical Society: Vienna, Austria, 2003; Volume 5, p. 02911.

40. Silva, P.G.; Michetti, A.M.; Guerrieri, L. Intensity Scale ESI 2007 for Assessing Earthquake Intensities. In *Encyclopedia of Earthquake Engineering*; Springer: Berlin/Heidelberg, Germany, 2015; pp. 1219–1237. [CrossRef]

41. Wells, D.L.; Coopersmith, K.J. New Empirical Relationships among Magnitude, Rupture Length, Rupture Width, Rupture Area and Surface Displacement. *Bull. Seismol. Soc. Am.* **1994**, *84*, 974–1002. [CrossRef]

42. Serva, L. An analysis of the world major regulatory guides for nuclear power plant seismic design. *Energ. Nucl.* **1993**, *10*, 77–96.

43. Silva, P.G.; González-Hernández, F.M.; Goy, J.L.; Zazo, C.; Mörner, N.A. Quaternary reverse surface faulting in Mallorca Island (Baleares, Spain). *Geogaceta* **1999**, *26*, 99–102.

44. Silva, P.G.; Rodríguez-Pascua, M.A.; Giner-Robles, J.L.; Pérez-López, R.; García-Tortosa, F.J.; Gómez Vicente, P.; Bardají, T.; Perucha, M.A.; Huerta, P.J.; Lario, J.; et al. *Catálogo de los Efectos Geológicos de los Terremotos de España*, 2nd ed.; Revisada y Ampliada; Riesgos Geológicos y Geotecnia 6; IGME: Madrid, Spain, 2019; 804p. (In Spanish)

45. Rodríguez-Pascua, M.A.; Pérez-López, R.; Silva, P.G.; Giner-Robles, J.L.; Garduño-Monroy, V.H.; Reicherter, K. A Comprehensive Classification of Earthquake Archaeological Effects (EAE) for Archaeoseismology. *Quat. Int.* **2011**, *242*, 20–30. [CrossRef]

46. González-Hernández, F.M.; Goy, J.L.; Zazo, C.; Silva, P.G. Tectónica Cuaternaria en la Cuenca de Palma (Isla de Mallorca): Análisis geomorfológico y neotectónico de la Falla de Cap d'Enderrocat. In *Actas V Reunión de Cuaternario Ibérico*; SGP—GTPEQ—AEQUA: Lisboa, Portugal, 2001; pp. 41–44.